A STUDY ON MIXED CONVECTION HEAT TRANSFER THROUGH A CHANNEL PARTIALLY FILLED WITH POROUS MEDIUM

A Thesis Submitted to
the Graduate School of Engineering and Sciences of
İzmir Institute of Technology
in Partial Fulfillment of the Requirements for the Degree of

MASTER OF SCIENCE

in Mechanical Engineering

by
Hasan ÇELİK

July, 2012
İZMİR

We approve the thesis of **Hasan ÇELİK**

Examining Committee Members:

Assoc. Prof. Dr. Moghtada MOBEDİ
Department of Mechanical Engineering
İzmir Institute of Technology

Assist. Prof. Dr. Ünver ÖZKOL
Department of Mechanical Engineering
İzmir Institute of Technology

Prof. Dr. M. Barış ÖZERDEM
Department of Energy Systems Engineering
Bahçeşehir University

13 July 2012

Assoc. Prof. Dr. Moghtada MOBEDİ
Supervisor, Department of Mechanical Engineering
İzmir Institute of Technology

Prof. Dr. Metin TANOĞLU
Head of the Department of
Mechanical Engineering

Prof. Dr. R. Tuğrul SENGER
Dean of the Graduate School of
Engineering and Sciences

ACKNOWLEDGEMENTS

I would like to thank and express my sincere gratitude to Dr. Moghtada MOBEDİ for his valuable advises and effort on my thesis. It was a pleasure for me to study under his supervising and guidance. His advices have enlightened my academic career, for sure.

I would like to express all my respect and sincere gratitude to Dr. Ünver ÖZKOL, Dr. Zafer İLKEN and Dr. Seçil ARTEM. I am pretty sure this thesis wouldn't be same without their inspiring lectures.

I would like to thank to my father for his great effort on my career. I am proud of being a member of the same chamber with you. You are the best mechanical engineer I have ever known.

I would like to express my gratitude to my mother. Without your everlasting support, I would never be as I am. Your support gives me the strength to overcome every difficulty I come up with in my life.

I also believe that my first advisor in my life, my grandmother, deserves the best words for her valuable advises. We miss you, rest in peace.

It is impossible to forget members of Fluid Mechanics Lab. Thank you very much for your hospitality at your laboratory during my visits to Izmir Institute of Technology.

Last but definitely not least, I would like to thank to my friends for their friendship and their valuable comments on my topic.

ABSTRACT

A STUDY ON MIXED CONVECTION HEAT TRANSFER THROUGH A CHANNEL PARTIALLY FILLED WITH POROUS MEDIUM

A study on mixed convection heat transfer in a laminar, fully developed, vertical channel is performed for three different cases: i) clear fluid channel ii) saturated porous medium filled channel iii) partially porous medium filled channel. For the all analyzed cases, motion and heat transfer equations are solved both analytically and numerically. The governing equations are presented both in dimensional and dimensionless forms. The dimensional forms of the governing equations are solved by numerical method while dimensionless equations are solved analytically. The dimensional results, obtained by numerical method, are converted into dimensionless values and compared with dimensionless results of analytical solutions. Good agreement between analytical and numerical results is observed. Based on the obtained results, velocity and temperature profiles are plotted for different values of Gr/Re, Da and porous layer thickness. A detailed discussion is performed on the obtained results. Moreover, heatline functions are obtained and plotted for different values of Gr/Re, Da and Peclet number. It is found that flow reversals in the channel highly depends on Gr/Re value and flow reversals occurs in the channel if Gr/Re exceeds threshold value. It is also found that for low Peclet numbers (i.e., Pe = 0.01), the path of heat flow is independent of Gr/Re and Darcy number. However, for high Peclet numbers (i.e., Pe = 5), the ratio of Gr/Re, Darcy number and thermal conductivity ratio influence heatline patterns, considerably.

ÖZET

KISMEN GÖZENEKLİ YAPI İLE DOLDURULMUŞ BİR KANALDA KARIŞIK ISI TAŞINIMI ÜZERİNE BİR ÇALIŞMA

Bu çalışma; tam gelişmiş, laminar, dik bir kanalda karışık taşınım için üç farklı durum üzerine yapılmıştır: i)akışkanla dolu kanal ii) gözenekli ortamla doldurulmuş kanal, iii) kısmen gözenekli ortamla doldurulmuş kanal. Momentum ve ısı transferi denklemleri her durum için analitik ve nümerik olarak çözülmüştür. Çalışmada, momentum ve ısı transferi denklemleri boyutlu ve boyutsuz olarak verilmiştir. Boyutlu momentum ve ısı transferi denklemleri nümerik olarak; boyutsuz momentum ve ısı transferi denklemleri ise analitik olarak çözülmüştür. Nümerik çalışma sonucu elde edilen boyutlu denklemlerin sonuçları, boyutsuz hale dönüştürülerek analitik sonuçlar ile karşılaştırılmıştır ve analitik ile nümerik sonuçların birbiri ile örtüştüğü görülmüştür. Elde edilen sonuçlara göre, hız ve sıcaklık profilleri değişik Gr/Re, Da ve gözenekli ortam kalınlıkları için çizilmiş ve yorumlanmıştır. Ayrıca ısının akışı denklemleri elde edilmiş ve farklı Gr/Re, Da ve Peclet değerleri için çizilmiştir. Ters akışların Gr/Re değerine oldukça bağlı olduğu görülmüş ve belli bir Gr/Re değeri aşıldığında ters akışların ortaya çıktığı gözlemlenmiştir. Ayrıca düşük Peclet değerlerinde ısı akışının Gr/Re değerinden bağımsız olduğu elde edilmiştir. Ancak yüksek Peclet değerlerinde hız profili,Gr/Re ve Da değeri ve akışkan ile gözenekli ortam ısı iletim katsayıları oranı ısı akış yönünü oldukça etkilemektedir.

TABLE OF CONTENTS

LIST OF FIGURES

Figure **Page**

LIST OF TABLES

Table **Page**

LIST OF SYMBOLS

b	spacing between walls (m)
C_p	specific heat, $JKg^{-1} K^{-1}$
g	acceleration due to gravity (ms^{-2})
Gr_c	Grashof number for channel with clear fluid
Gr_p	Grashof number for channel with porous media
h	heatfunction, Wm^{-1}
H	dimensionless heatfunction
J	heat flux vector, $Wm^{-2}K^{-1}$
k	thermal conductivity, $Wm^{-1}K^{-1}$
K	permeability (m^2), thermal conductivity ratio
M	relative viscosity, μ/μ_{eff}
p	pressure (Pa)
P	dimensionless pressure
Pe	Peclet number
Re	Reynolds number
S	shape parameter, $\sqrt{M / Da}$
T	temperature (^oC)
u, v	axial and transverse velocity, (ms^{-1})
U, V	dimensionless axial and transverse velocity
x, y	axial and transverse coordinate, (m)
X, Y	dimensionless axial and transverse coordinate

Greek Symbols

β	coefficient of thermal expansion
θ	dimensionless temperature
Γ	pressure gradient along channel
μ	dynamic viscosity of the fluid ($kgms^{-1}$)
μ_{eff}	dynamic viscosity for Brinkman's model ($kgms^{-1}$)
ν	kinematic viscosity of the fluid (m^2s^{-1})
ρ	density (kgm^{-3})

Subscripts

c	cold wall , clear fluid
eff	effective
f	fluid
i	interface
p	porous
h	hot wall
av	average
ref	reference value

CHAPTER 1

INTRODUCTION

A material consisting of finite volume solids with interconnected voids can be called as porous medium. Beach sand, human lungs and wood can be given as examples of porous medium. Researches in heat and mass transfer in porous media has been increased due to importance of the subject in many engineering applications. A sample of porous medium can be seen in Figure 1.1.

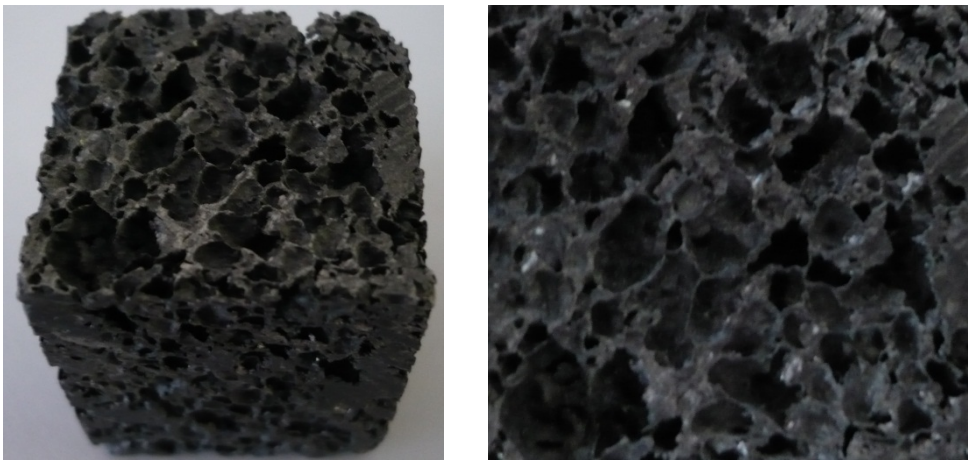

Figure 1.1. Porous media

Porous media provide enhancement of heat transfer in convection problems. The following comments may explain this issue better. As it is known, the Newton's Law of Cooling is:

$$Q = hA(T - T_{ref}) \tag{1.1}$$

where Q is total heat transfer rate (W), h is convective heat transfer coefficient (W/m^2K), A (m^2) is the heat transfer area and T and T_{ref} (K) are the temperature of fluid and free stream respectively. As seen from the Equation 1.1, the increase of convective heat transfer coefficient and/or heat transfer area and/or increase of temperature difference between the fluid and reference can enhance heat transfer. There are several

techniques to effect these parameters to enhance heat transfer such as use of fins, jet impingement, fluid vibration or porous media.

The use of a porous medium might be very effective way to enhance heat transfer. There are several reasons for enhancing of heat transfer by using a porous medium. First of all, a porous medium increases heat transfer area. Thus, the total heat transfer is increased as it was mentioned. Secondly, a porous medium generates fluctuations and mixed fluid flow. These fluctuations provide the increase of heat transfer coefficient and consequently heat transfer rate increases. Third of all, a porous medium can increase diffusion heat transfer if a high conductive porous medium is used in the system. The use of high conductive porous medium increases the heat conduction in flow field.

Heat is transferred due to random molecular motion, diffusion, as well as macroscopic or bulk motion of the fluid where bulk motion represents a motion of large number of molecules collectively. This bulk motion, advection, contributes to heat transfer if temperature gradient occurs. Therefore, total heat transfer can be explained as a superposition of energy transport by random motion and by bulk motion or in other words by convection. Therefore, convection can be explained as energy transfer between a solid surface and a fluid in motion (Incropera and DeWitt (2007)).Nature of the flow is widely used to classify convection heat transfer. If the flow is caused by external means such as fan, pump etc. convection is called forced convection (Figure 1.2(a)). The buoyancy forces which are a result of density differences due to temperature variation in fluid can be neglected in forced convection. However, if the motion of fluid is caused by buoyancy forces, convection is called as natural convection (Figure 1.2(b)). If both natural and forced convection heat transfer conjugates each other in situations like the velocity of the flow of external means is small and buoyancy forces are high, this heat transfer situation, where the importance of natural and forced convection are competent, is called as mixed convection.(Figure 1.2(c))**.** Mixed convection is an important heat transfer situation in applications where buoyancy forces exist and can change the flow pattern(Kakaç and Yener (1995)). For instance, although forced flow through rotating components such as rotor blades of turbines presents in means of centrifugal forces, these forces may provide natural convection flows and may change flow pattern due to temperature differences. Mixed convection is also important

in design of solar collectors. What is more, heat exchange in oil coolers is affected by natural convection on the forced flow (Kakaç and Yener (1995)).

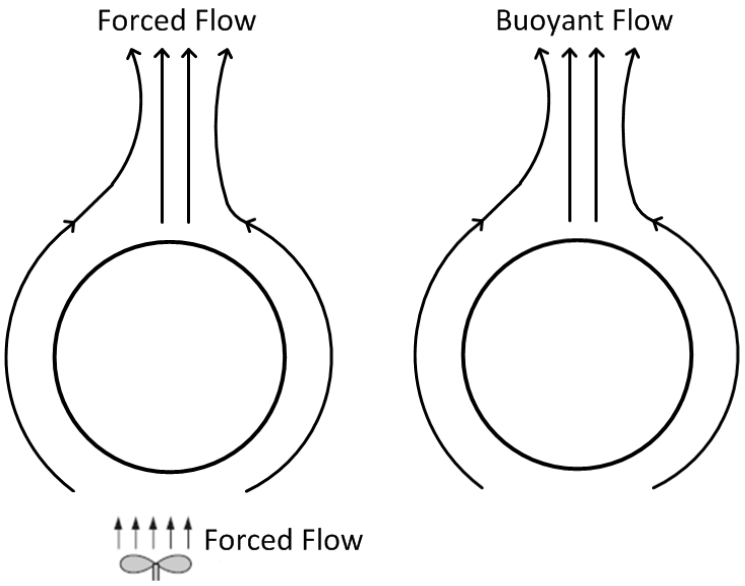

(a)

(b)

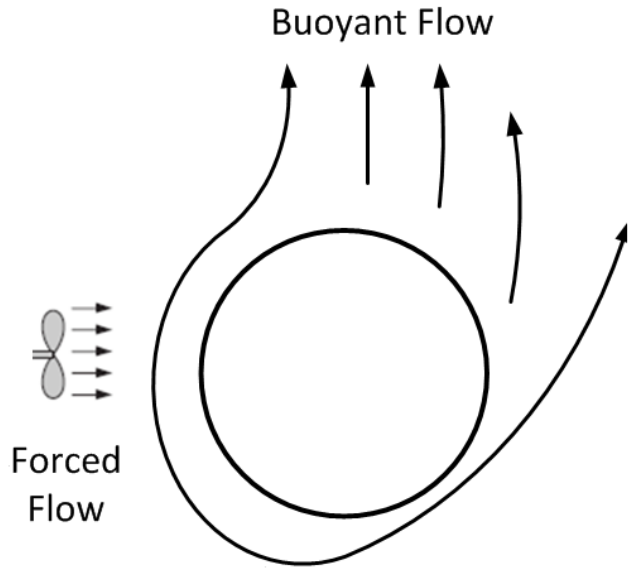

(c)

Figure 1.2. Convection mechanisms a) Forced convection b) Natural convection c) Mixed convection

Mixed convection may be aided or opposed to forced convection related to the forced motion as seen on Figure 1.3. If the buoyant motion is in the same direction with

the forced motion, then the flow is called buoyancy-aided flow which enhances heat transfer rate. However, if the buoyant motion is in the opposite direction with the forced motion, the flow is called buoyancy-opposed flow which hurts heat transfer rate.

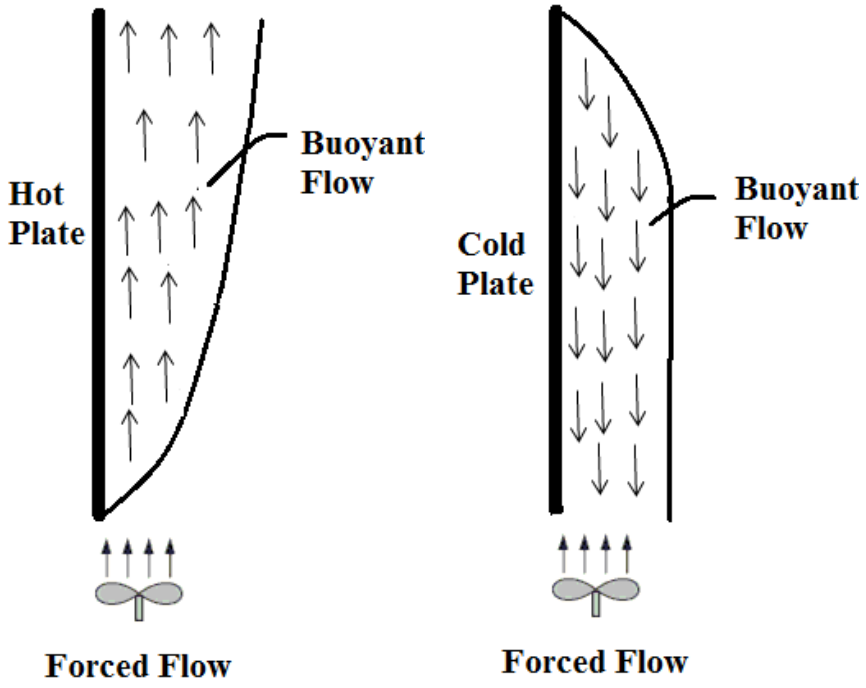

a) b)

Figure 1.3. Types of mixed convection a) aided b) opposing

Convection problems can be divided into two groups as external and internal problems. External convection heat transfer occurs over a body, while internal convection forms inside a body. Convection heat transfer in ducts and channels are widely faced in industrial application such as heat exchanger designs. Heat transfer in a duct or channel can be divided into two regions as entrance and fully developed regions. The definition and determination of entrance region are given in heat transfer text books in details. However, for many applications when the channel is long, the effect of the entrance region can be neglected if heat transfer in entrance region is compared with the heat transfer of the whole channel/duct. That is why the analysis of fully developed heat and fluid flow has been performed by many researchers.

The concept of fully developed flow in channels with mixed convection is different than forced convection since velocity profiles depend on the temperature gradient in the channel. Fully developed mixed convection can appear in channels with

asymmetric boundary conditions. Flow reversal in fully developed mixed convection heat transfer in channels has an important effect on heat transfer from the walls. This flow may appear in a channel when the flow rate is fixed and the buoyancy effect cannot be neglected. Buoyancy effect is high at the region close to the hot wall which increases velocity in that region. Thus, a downward flow emanates from the open top of the channel and by this way flow reversal occurs.

The present study is aimed to investigate heat and fluid flow in a fully developed mixed convection channel partially filled with porous medium. The enhancement of heat transfer by using a porous layer is also analyzed for the considered channel. However, before attain to the main of this thesis, many cases are analyzed to be sure of the obtained results. The present study is started with investigating heat and fluid flow in a clear vertical channel whose walls are at different temperatures. Two different studies as dimensional and dimensionless are performed for analyzing the heat and fluid flow in a clear channel. Constant wall temperatures are applied at both sides of the channel. The studies for clear channel are presented in Chapter 4 and 5. Heat and fluid flow in fully porous vertical channel is studied by dimensional and dimensionless approaches in Chapter 6 and 7, respectively. Finally, partially porous channel is studied by dimensional and dimensionless approaches in Chapter 8 and 9. Heatline functions are described for clear, fully porous medium and partially porous medium channels in Chapter 10. In Chapter 11, numerical solution procedure employed to solve heat transfer and motion equations is explained. The obtained results for the studies channels are made in Chapter 12. The performed study in this thesis is concluded in Chapter 13.

In this thesis, firstly, all governing equations are solved dimensionally for given cases. Then, the governing equations are solved dimensionless to find a general solution and make general conclusions. The main purpose of this thesis is to increase heat transfer rate along the channel.

CHAPTER 2

A REVIEW ON MIXED CONVECTION HEAT AND FLUID FLOW IN CHANNEL/DUCT

Several studies on mixed convection in a channel/duct filled with clear fluid, fully saturated porous medium and partially filled with porous medium were reported in literature. These studies are summarized in this chapter.

As it is mentioned in Chapter 1, the energy and fluid motion equations of fully developed mixed convection flow are different than the forced convection fully developed flow since the velocity changes with temperature in the channel. In a channel with fixed inlet mass flow, flow reversal may appear due to buoyancy effect. The buoyancy effect near the hot wall increases the fluid velocity in that region, and thus, a downward flow occurs from the open top of the channel. The first experimental evidence for its occurrence has been supplied by Sparrow, Chrysler, and Azevedo (1984). The initial flow analysis of mixed convection has been discussed in the work of Ostrach (1954), and Lietzke (1954).

Win Aung and Worku (1986) presented the results for mixed convection flows between parallel-plate channels in which the net through-flow rates are constant as shown in Figure 2.1. They assumed that the flow is fully developed. The mixed convection flow between parallel plates in which fixed flow rate is studied theoretically. They found that when the wall temperatures are unequal, a reversed flow situation occurs if the magnitude of the buoyancy parameter Gr/Re exceeds a certain threshold value. Here, Gr and Re are Grashof and Reynolds numbers and they are defined based on distance between vertical plates.

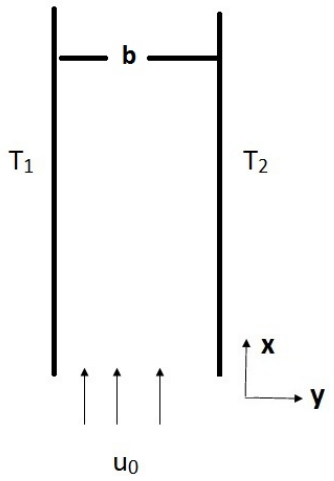

Figure 2.1. Schematic view of study of Aung and Worku (1986)

W. Aung and Worku (1987) has studied mixed convection in ducts with asymmetric wall heat fluxes. The studied domain is shown in Figure 2.2. They considered fully developed pure fluid flow channel with aiding buoyancy forces. They concluded that there are significant differences between uniform heat fluxes and uniform wall temperatures in mixed convection with asymmetrically heated vertical plates. They also provided that flow reversal is more prone to occur in asymmetric wall heating at uniform wall heat fluxes than asymmetric wall heating at uniform wall temperature.

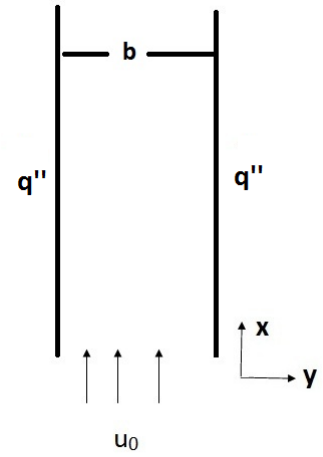

Figure 2.2. Schematic view of study of Aung and Worku (1987)

Parang and Keyhani (1987) investigated the boundary effects in a laminar mixed convection flow through an annular porous medium by using Brinkman-Extended

Darcy model. They aimed to clarify in which situations Brinkman term can be neglected in their study. They found that the Brinkman term has a negligible effect on the flow when Darcy number is very small.

The problem of aiding and opposing mixed convection in a vertical porous layer with a finite wall heat source was investigated by Lai et al. (1988). They studied two-dimensional, steady mixed convection in a vertical porous layer for the case when a finite isothermal heat source is located on one adiabatic vertical wall and the other vertical wall is isothermally cooled. They concluded that for the aiding flow, the slope of the Nusselt number curve increases with Peclet number unless the flow has approached the forced convection regime.

The combined free and forced convection of a fully developed Newtonian fluid within a vertical channel composed of porous media when the viscous dissipation effects are taken into consideration is studied by Al-Hadhrami et al. (2002) as their studied channel seen on Figure 2.3. The governing fourth-order, ordinary differential equation, which contains the Darcy and the viscous dissipation terms, is solved analytically using perturbation techniques and numerical method. They showed that the effect of the Darcy number decreases as the critical Rayleigh numbers increase.

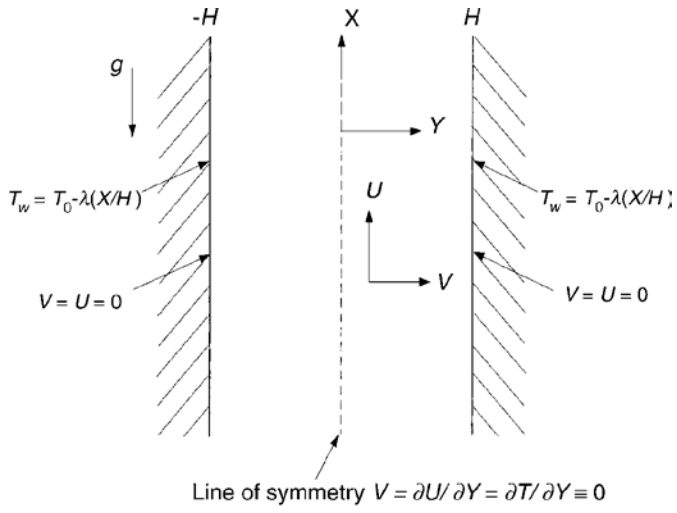

Figure 2.3. Schematic view of study of Al- Hadhrami et al. (2002)
(Source: Al-Hadhrami et al., 2002)

Umavathi et al. (2005) studied a numerical study of mixed convection in a vertical channel filled with porous media, as seen on Figure 2.4, including inertial forces. They considered isothermal-isothermal, isoflux-isothermal boundary conditions.

The governing equations are solved numerically by finite difference method with Southwell–Over–Relaxation technique for extended Darcy model and analytically using perturbation series method for Darcian model. They concluded that viscous forces enhance flow reversal in downward flow while it counters the flow in upward flow.

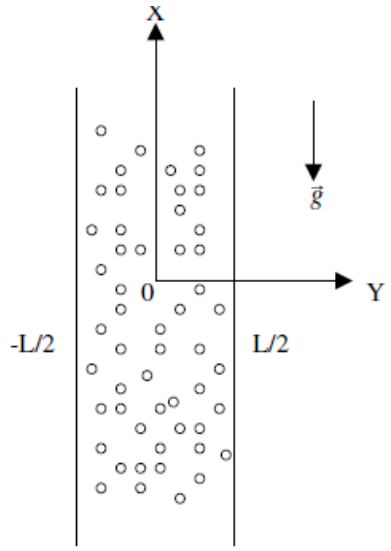

Figure 2.4. Schematic view of study of Umavathi et al.(2002)
(Source: Umavathiet al.,2005)

Mixed convection with viscous dissipation in a vertical channel filled with a porous medium, buoyancy aided and opposing flow is analyzed analytically with isothermal and isoflux boundary conditions by Barletta et al. (2007). The study was performed for fully developed flow as seen from Figure 2.5.They assumed that the Darcy law and the Boussinesq approximation hold, the effect of viscous dissipation is significant, and the average flow velocity U_m is prescribed. The Darcy and energy balance equations have been solved by an analytical series expansion method. The mechanical and thermal characteristics of the flow are investigated in this study. They concluded that upward or downward laminar flow solutions may exist as long as U_m does not exceed a maximum value.

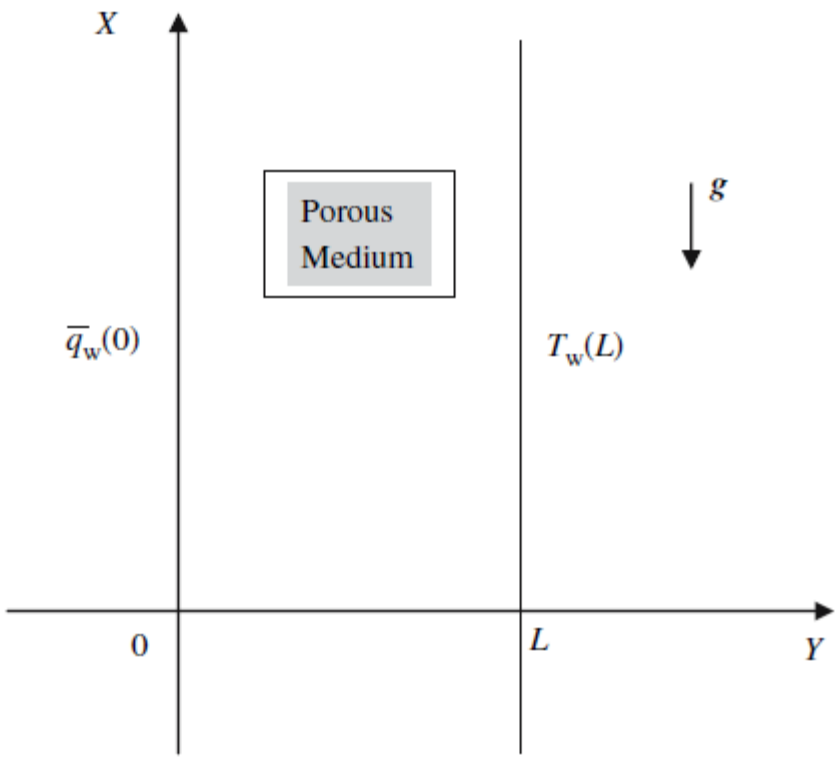

Figure 2.5. Schematic view of study of Barletta et al.(2007)
(Source: Barletta et al., 2007)

Buoyancy aided and opposing flow is analyzed numerically for a vertical porous channel with isothermal and isoflux boundary conditions in the case of a fully developed flow is studied by Barletta and Nield (2009), as seen on Figure 2.6. In their study, the effects of viscous dissipation and pressure work are taken into account in the framework of the Oberbeck–Boussinesq approximation scheme and of the Darcy flow model. Buoyant flow for a saturated porous layer is examined in fully developed parallel velocity field in their study. They concluded that for upward driven flows, the combined effects of viscous dissipation and pressure work may produce a net cooling of the fluid even in the case of a positive heat input from the isoflux wall. However, for downward driven flows, viscous dissipation and pressure work yield a net heating of the fluid.

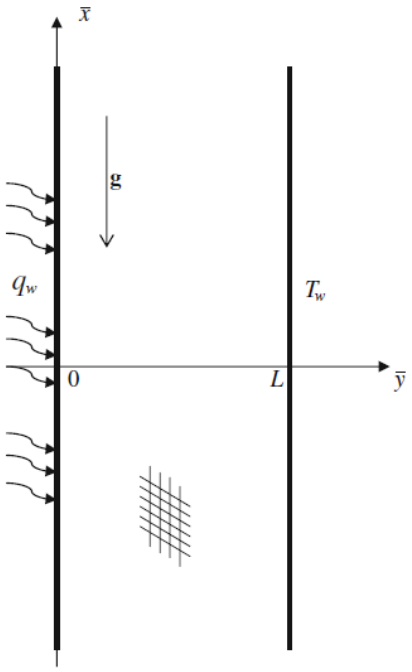

Figure 2.6. Schematic view of study of Barletta and Nield(2009)
(Source: Barletta and Nield, 2009)

Chang and Chang (1995) numerically analyzed the developing mixed convection in a vertical tube partially filled with porous medium which is demonstrated on Figure 2.7. Inertia and boundary effects are included in this study. They concluded that the hydrodynamic enhance length is shorter as the value dimensionless porous layer thickness is increased, and is longer as the values of Darcy and Grashof dimensionless numbers are increased. The thermal entrance becomes longer as the values of dimensionless porous layer thickness and Darcy number increase and shorter as the values of Gr increase.

An analysis of mixed convective flow in partially filled porous channel is studied by Kumar et al. (2009) as seen on Figure 2.8. Three types of thermal boundary conditions such as isothermal–isothermal, isoflux–isothermal, and isothermal–isoflux for the left–right walls of the channel are considered. They studied velocity and temperature distribution in the channel in their paper.

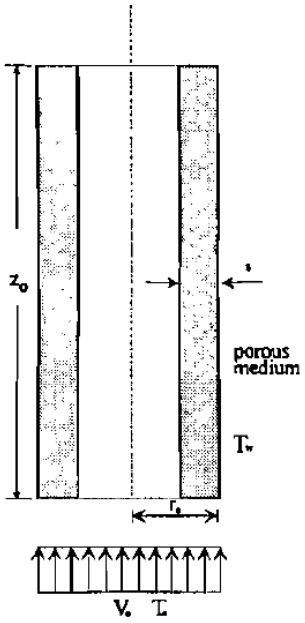

Figure 2.7. Schematic view of study of Chang and Chang
(Source: Chang and Chang, 1995)

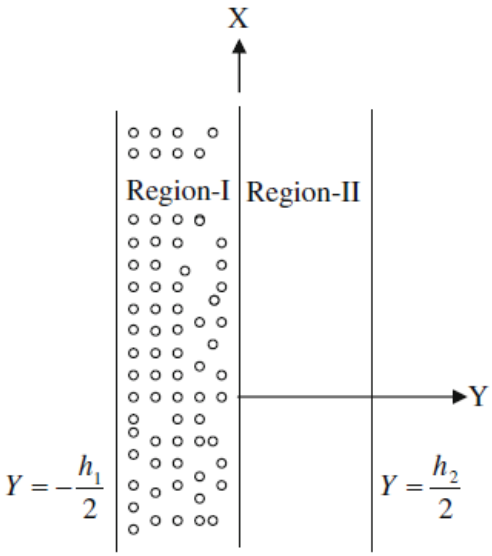

Figure 2.8. Schematic view of study of Kumar et al.(2009)
(Source: Kumar et al., 2009)

Isotherms and streamlines are widely used in convective heat transfer studies in order to describe heat and fluid flow in a domain. However, understanding of heat flow direction is not easy by using isotherms and streamlines. That is why, heatline technique was proposed by Kimura and Bejan (1983) to observe path of heat flow. The heatline visualization technique can be employed to observe not only path of heat flow but also

intensity of heat flux at any location of domain for a convection and/or conduction steady or unsteady heat/mass transfer problems.

Costa (1999) reviewed studies on heatline visualization technique and summarized its application. He concluded that the heat and mass functions conjugated problems, as well as the stream-function problem can be derived using a common physical procedure and such problems are formally similar.

Hakyemez et al. (2008) and Mobedi (2008) used the heatline technique to observe heat transport in the entire domain of a square cavity with thick horizontal walls. In their study, the vertical walls of the enclosure are differentially heated and the horizontal walls are adiabatic. They used heatline technique to visualize heat transport. In the study of Mobedi (2008), the effect of conduction of horizontal walls on natural convection heat transfer in a square cavity, as seen on Figure 2.9(b), is numerically investigated. The vertical walls of the cavity are at different constant temperatures while the outer surfaces of horizontal walls are insulated. Usefulness of heatline visualization technique for conjugate heat transfer problems is showed in this study.

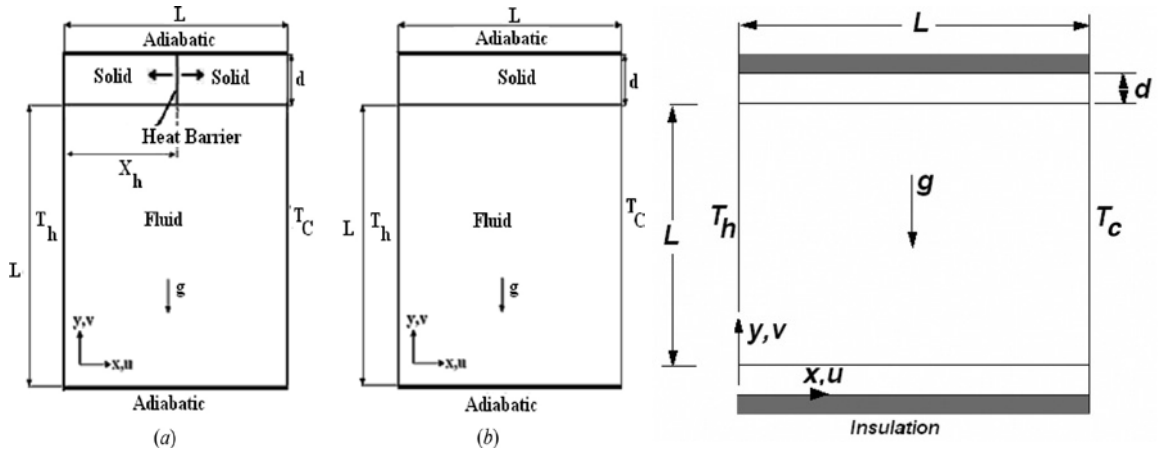

(a) (b)

Figure 2.9. Schematic view of study of a) Hakyemez et al. (2008) b) Mobedi (2008) (Source: Hakyemez et al. 2008 ; Mobedi 2008)

Mobedi et al. (2010) also divided heatfunction equation into the diffusion and convection heatfunctions by using superposition rule. They used superposition rule to obtain the mathematical definitions of diffusion and convection heatfunctions and corresponding boundary conditions. They concluded that based on the distribution of total heatlines, two regions are detected in the cavity, an active region with the positive values of heatlines signifying dominant conduction heat transfer and a passive region

with the negative heatfunction values in where convection heat flow is dominant and heat only rotates in a closed contour pattern.

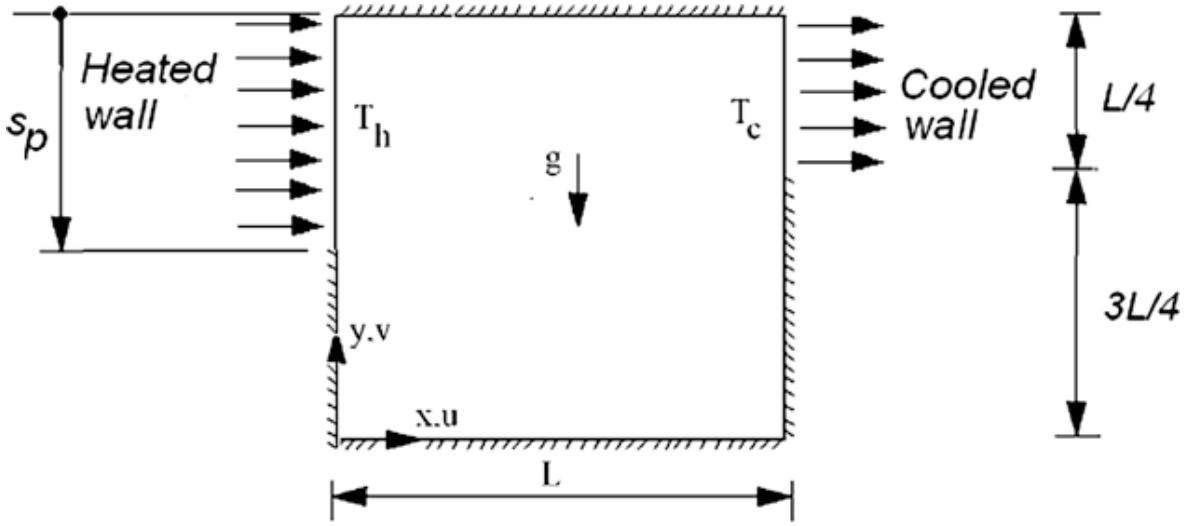

Figure 2.10. Schematic view of study of Mobedi et al.
(Source: Mobedi et al., 2010)

Varol et al. (2010) used heatline patterns to study natural convection heat transfer of cold water near 4 ^{o}C in a thick bottom walled cavity filled with a porous medium, as seen on Figure 2.11, numerically. In their study, they assumed the cavity is isothermally heated from the outside of the thick bottom wall and cooled from ceiling. They concluded that the increase of Rayleigh number and thermal conductivity ratio increases heat transfer through the cavity. However, the increase of thickness of the bottom wall reduces the mean Nusselt number.

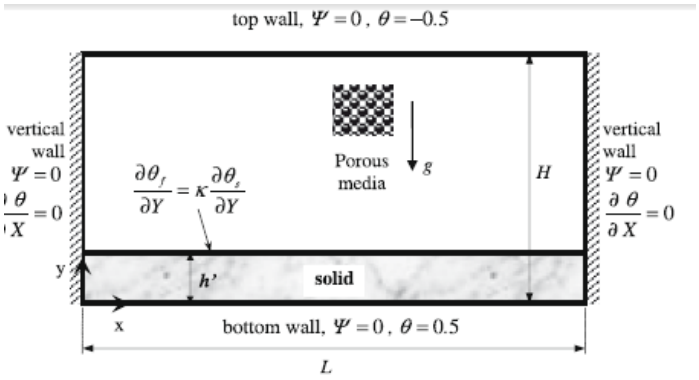

Figure 2.11. Schematic view of study of Varol et al.
(Source: Varol et al., 2010)

Kaluri et al. (2009) performed a numerical study on heat distribution and thermal mixing for steady laminar natural convective flow within fluid-saturated porous square cavities by using heatline technique. They considered three different cases; firstly uniformly heated bottom wall, then discrete heat sources on walls and finally uniformly heated left and bottom walls. They found that distributed heating enhances heat distribution and thermal mixing compared to uniform heating case. Their studied domain is demonstrated in Figure 2.12.

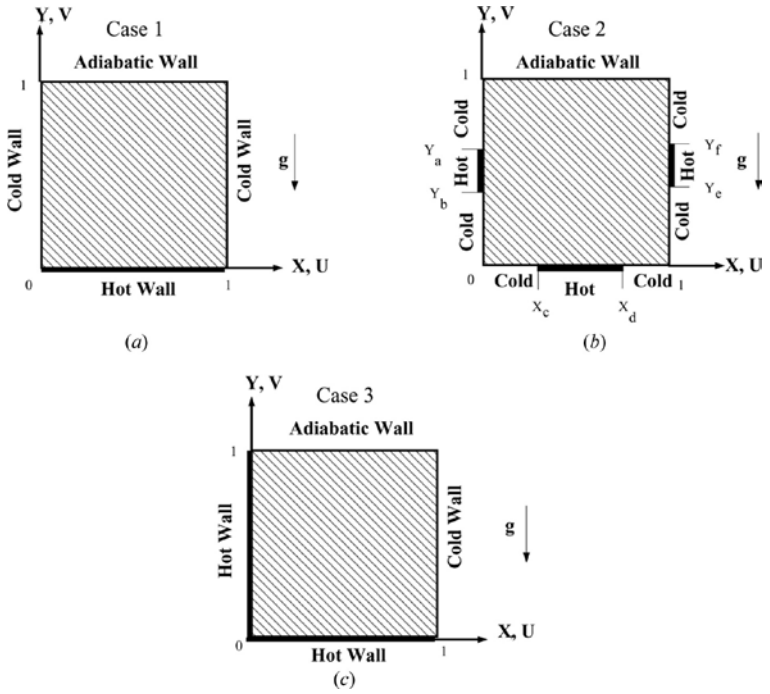

Figure 2.12. Schematic view of study of Kaluri et al.
(Source: Kaluri et al. 2009)

Basak et al. (2010), Kaluri and Basak (2010) and Kaluri et al. (2010) performed several studies on heat transport field for various domains under different boundary conditions.

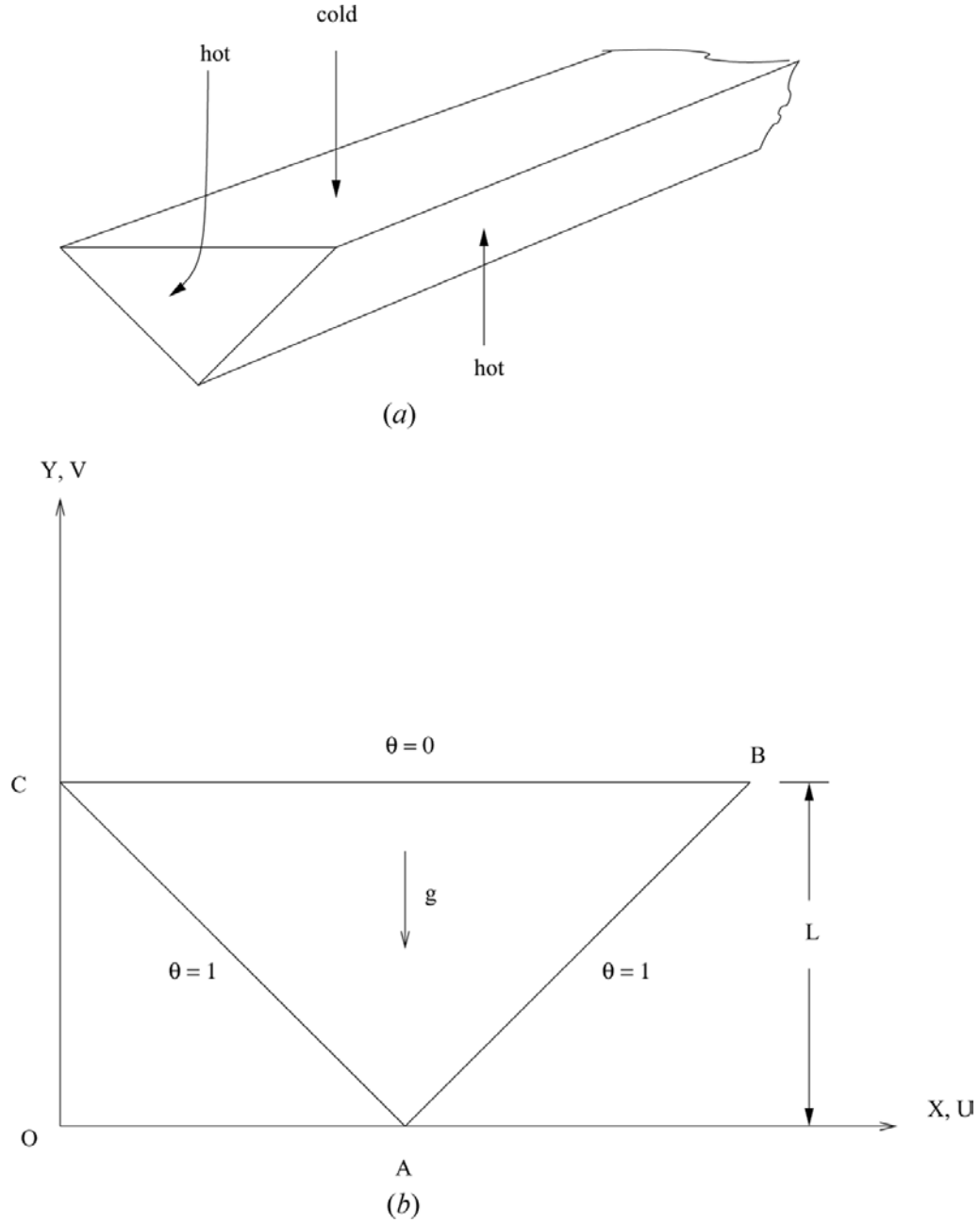

Figure 2.13. Schematic view of study of Basak et al.
(Source: Basak et al. 2010)

In the study of Basak et al. (2010), Figure 2.13, natural convection in a porous triangular cavity has been analyzed. They used finite element method to solve governing equations. They provided heat transfer analysis in terms of local and average Nusselt numbers. They concluded that the local Nusselt number for the side wall is low at the intersection point of hot walls and high at the intersection point of the hot and cold walls.

Kaluri et al. (2010), Figure 2.14, studied Natural convection in right-angled triangular enclosures with various angels via heat flow analysis for various uniform isothermal and linear isothermal heating thermal boundary conditions. They visualized heatline patterns under different conditions. They provided effect of increase in angle heat flux at top vertex decreases.

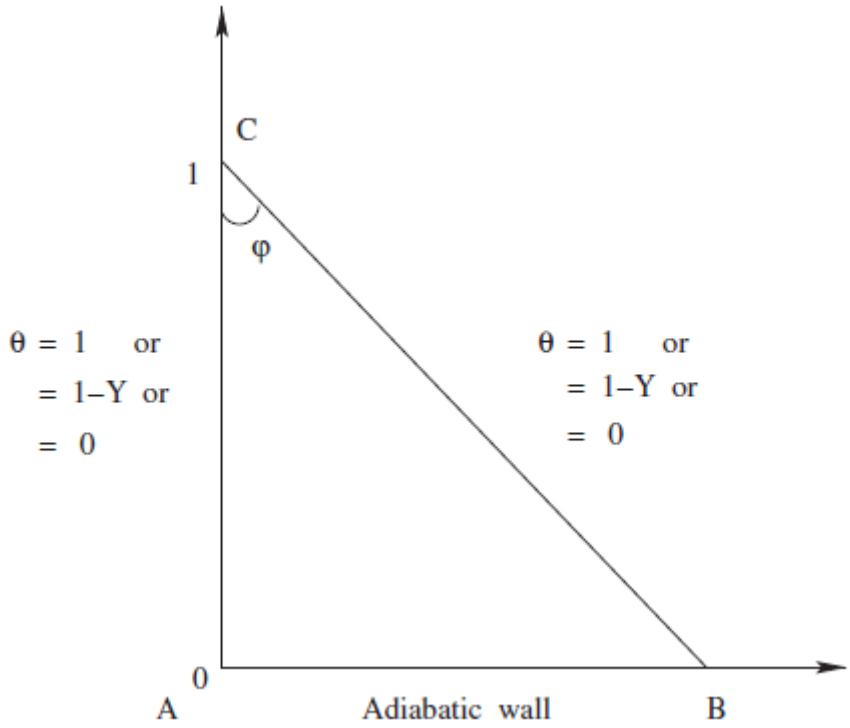

Figure 2.14. Schematic view of study of Kaluri et al.
(Source: Kaluri et al. 2010)

Waheed (2009) studied the problem seen on Figure 2.15 of the natural laminar convection in square enclosures filled with fluid-saturated porous medium by using the heatfunction formulation approach. The Brinkman-extended Darcy equations of motion, energy, and heatfunction equations were solved by the finite-difference method in the study. It is concluded that problem governing parameters have strong effect on the convection strength, isotherms, and heatfunction fields and profiles. What is more, an increase in the value of the Darcy number above unity has no more influence on the heatfunction profiles.

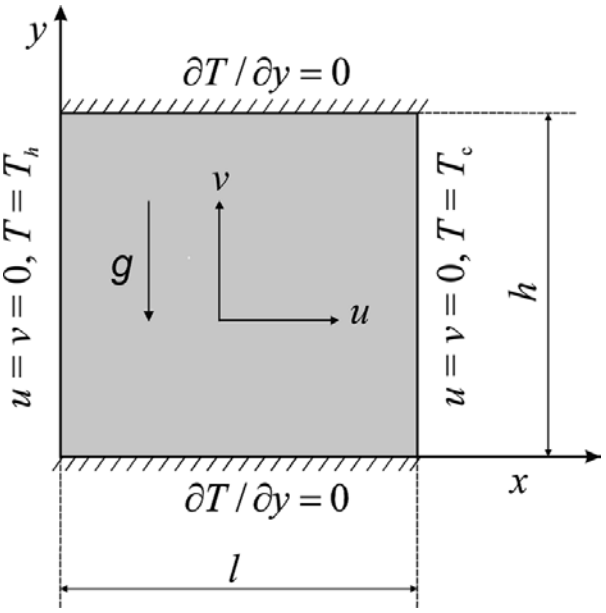

Figure 2.15. Schematic view of study of Waheed
(Source: Waheed 2009)

The above literature review reveals that the most of studies on visualization of heat flow were performed on the closed spaces such as closed cavities rather channels and ducts. Probably, the first study on observation of heat transport path in a channel was performed by Morega and Bejan (1993).

CHAPTER 3

FUNDAMENTAL CONCEPTS

As it is described in Chapter 1, finite volume solids with interconnected voids called as porous media. Studies on porous media are rising due to its importance in nature science and industrial applications. Convection in porous media also has many application areas in many technologies. These technologies include oil recovery, nuclear waste disposal, insulation of buildings, drying processes, nuclear reactors, solar systems, geothermal reservoirs, porous journal bearings, modern electronic equipment and heat exchangers.

3.1. Porosity

Porosity, ε, is defined as the ratio of volume occupied by the fluid to the total volume of the porous medium.

$$\varepsilon = \frac{V_f}{V_{total}} \tag{3.1}$$

In defining of porosity, all the void space is assumed to be connected each other. If any discontinuity in connection between void appears in the medium then effective porosity, which can be explained as the ratio of connected void to total volume, should be introduced to the study. The porosity is mostly between 0.2 and 0.6 for natural media. However, this value approaches to 1 by man-made materials such as foams (Nield and Bejan (2006)).

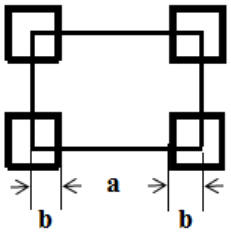

Figure 3.1. A sample of porous media

A sample calculation for determination of porosity for a square bar porous media shown in Figure 3.1 can be done as;

$$\varepsilon = \frac{(a+2b)^2 - 4b^2}{(a+2b)^2} \tag{3.2}$$

3.2. Permeability

Permeability, K, is a coefficient in dimension of m^2. Although permeability is independent of nature of the fluid, geometric structure of the porous medium is highly dependent factor of permeability. The increase in permeability provides a fluid flow similar to a clear medium. The values of permeability vary widely depending on the porous material. Similar to effective porosity, effective permeability should be introduced to the study if any discontinuity between voids appears.

As permeability depends on the geometry inside the porous medium, the equation to calculate permeability differs for all geometry. In this thesis, porous medium consists of large numbers of square bar is considered in Chapter 6 and 8. The relation used to calculate for the aforementioned porous medium is:

$$K = \frac{\varepsilon^3 2b^2}{120(1-\varepsilon)^2} \tag{3.3}$$

3.3. Fluid Motion Equation for Porous Media

There are several fluid motion equations for studying of fluid flow in a porous medium. In the following subsection these equations are discussed.

3.3.1. Darcy's Law

Henry Darcy's studies into hydrogeology stated that the volume averaged fluid velocity through a column of porous media is directly proportional to the pressure gradient established along the column and the permeability of the space and inversely proportional to the viscosity of the fluid. This equation for mixed convection can be written as;

$$u = \frac{K}{\mu}\frac{\partial P}{\partial x} + \rho g \tag{3.4}$$

where K is permeability and μ is dynamic viscosity. In three dimensions, Darcy's Law can be expressed as;

$$\mathbf{u} = \frac{\mathbf{K}}{\mu}\nabla P + \rho g \tag{3.5}$$

where K is second order tensor. It should be mentioned that ρg represents the effect of buoyancy force. It is negligible for forced convection; however this term should be taken into account for natural and mixed convection problems.

3.3.2. Brinkman-Extended Darcy's Law

Darcy's Law fails when boundary effects are important. (i.e. internal flows) Therefore, additional terms for boundary conditions are needed to be included into fluid motion equation. Thus, a new variable depends on the fluid and structure of the porous medium, effective dynamic viscosity, μ_{eff} should be introduced to the fluid motion equation.

$$\mu_{eff}\frac{d^2u}{dy^2} - \frac{\mu}{K}u - \frac{dp}{dx} + \rho g = 0 \tag{3.6}$$

where μ_{eff} is effective dynamic viscosity . There are many studies on determination of effective dynamic viscosity. One of the common relations for determination of effective dynamic viscosity is:

$$\mu_{eff} = \frac{1}{\varepsilon} \tag{3.7}$$

The general form of Brinkman-Extended Darcy's Law is:

$$\mu_{eff}\nabla\mathbf{u} - \frac{\mu}{K}\mathbf{u} - \nabla P + \rho g = 0 \tag{3.8}$$

3.3.3. Forchheimer - Brinkman Extended Darcy's Law

Darcy's Law may not be appropriate when inertial forces are not negligible because Darcy's Law is only function of pressure gradient and viscous effects. For high velocity fluid flow in the porous medium, the inertia effect should be included. Thus, a modification is needed to be made to include inertial forces. Forchheimer – Brinkman Extended Darcy's Law can be written as follows;

$$\mu_{eff}\frac{d^2u}{dy^2}-\frac{C}{\sqrt{K}}\rho_f u^2-\frac{\mu}{K}u-\frac{dp}{dx}+\rho g=0 \tag{3.9}$$

where C is Forchheimer constant, K is permeability, μ is dynamic viscosity. Second term stands for inertial contribution while third is viscous contribution. For three dimensions, Forchheimer equation can be written as;

$$\mu_{eff}\nabla^2\mathbf{u}-\frac{C}{\sqrt{K}}\rho_f \mathbf{u}^2-\frac{\mu}{K}\mathbf{u}-\nabla\mathbf{P}+\rho\mathbf{g}=0 \tag{3.10}$$

3.4. Heat Flow in Porous Media

According to the first law of thermodynamics, the total energy in the system should be conserved. Therefore, energy balance can be written as follows when a thermal equilibrium exists between fluid and solid in the porous media.

$$\rho C_p\mathbf{u}\nabla\mathbf{T}=k_{eff}\nabla^2\mathbf{T} \tag{3.11}$$

where T is the average temperature of the solid and fluid for a small volume inside the porous media. k_{eff} is effective thermal conductivity for fluid and solid porous material which can be calculated as follows;

$$k_{eff}=\varepsilon k_f+(1-\varepsilon)k_s \tag{3.12}$$

3.5. Compatibility

Definition of mean temperature is used to derive compatibility condition. Mean temperature equation is seen on Equation (3.13);

$$T_m = \frac{\int_0^b \rho C_p u T dy}{\int_0^b \rho C_p u dy} \tag{3.13}$$

As density and constant pressure specific heat of the fluid is assumed constant and can be taken out of integral. Therefore, Equation (3.13) can be written as;

$$T_m = \frac{\int_0^b u T dy}{\int_0^b u dy} \tag{3.14}$$

Using definition of mean velocity;

$$u_m = \frac{\int_0^b u dy}{\int_0^b dy} = \frac{\int_0^b u dy}{b} = \int_0^b u dy = b u_m \tag{3.15}$$

Therefore, Equation (3.14) turns into;

$$T_m = \frac{\int_0^b u T dy}{b u_m} \tag{3.16}$$

Using normalized velocity definition, $\hat{u} = \frac{u}{u_m}$, Equation (3.16) can be written as;

$$b T_m = \int_0^b \frac{u}{u_m} T dy = \int_0^b \hat{u} T dy \tag{3.17}$$

Using dimensionless parameters in Equation (3.18), Equation (3.17) turns into Equation (3.19);

$$\theta = \frac{T - T_s}{T_m - T_s}, \; y = \frac{Y}{b} \tag{3.18}$$

$$T_m = (T_m - T_s)\int_0^1 \hat{u}\theta dY + T_s \int_0^1 \hat{u} dY \tag{3.19}$$

where

$$\int_0^1 \hat{u} dY = \frac{\int_0^1 u dY}{u_m} = \frac{\int_0^1 u dY}{\int_0^1 u dY} = 1 \tag{3.20}$$

Therefore, using Equation (3.20) in Equation (3.19), compatibility condition can be found as follows;

$$\int_0^1 \hat{u}\theta dY = 1 \tag{3.21}$$

CHAPTER 4

FULLY DEVELOPED MIXED CONVECTION IN A CHANNEL WITH PURE FLUID: DIMENSIONAL GOVERNING EQUATIONS

4.1. Definition of the Problem

Mixed convection between a two vertical parallel plate filled with a clear, incompressible fluid is considered. The fluid is assumed to be Newtonian and incompressible, while the flow is laminar, thermally and hydro-thermally fully developed and steady. The channel has a rectangular cross-section with width of b. It is assumed that the plates are infinitely long in z direction, x is being vertical direction and y is perpendicular direction to x direction. It is also assumed that the flow in the channel is fully developed, unidirectional and steady. The fluid properties are constant except the density in buoyancy term of the momentum equation. Viscous dissipation is neglected for this case. A constant temperature is applied to the walls of the channel as shown in Figure 4.1 and also gravity acts in x-direction.

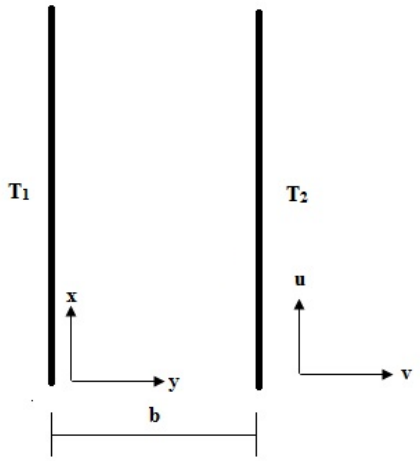

Figure 4.1. Considered problem

4.2. Governing Equations

The governing equations, continuity, momentum and heat transfer equations, is explained in this section.

4.2.1. Continuity Equation

The general form of the continuity equation for incompressible flow can be expressed as;

$$\vec{\nabla} \cdot \vec{V} = 0 \tag{4.1}$$

Hence, continuity equation for the case mentioned in Section 4.1 can be written for rectangular coordinates;

$$\frac{d\,u}{d\,x} = 0 \tag{4.2}$$

4.2.2. Momentum Equation

To obtain velocity field, Navier-Stokes equation in x and y directions are needed to be solved simultaneously. The general form of Navier-Stokes equations can be expressed as;

$$u\frac{\partial u}{\partial x} + v\frac{\partial u}{\partial y} = -\frac{1}{\rho}\frac{\partial P}{\partial x} + \nu\left(\frac{\partial^2 u}{\partial x^2} + \frac{\partial^2 u}{\partial y^2}\right) + \rho g\beta(T - Tav) \tag{4.3}$$

$$u\frac{\partial v}{\partial x} + v\frac{\partial v}{\partial y} = -\frac{1}{\rho}\frac{\partial P}{\partial y} + \nu\left(\frac{\partial^2 v}{\partial x^2} + \frac{\partial^2 v}{\partial y^2}\right) \tag{4.4}$$

Navier-Stokes equation can be reduced under the assumptions mentioned in section 4.1 as;

$$\mu\frac{d^2 u}{d\,y^2} - \frac{dP}{dx} + \rho g\,\beta\,(T - T_{av}) = 0 \tag{4.5}$$

where T_{av} is average temperature of the left and right plates.

$$\frac{\partial P}{\partial y} = 0 \tag{4.6}$$

4.2.3. Heat Transfer Equation

General form of energy equation can be written as;

$$(\rho C_p)(u\frac{\partial T}{\partial x} + v\frac{\partial T}{\partial y}) = k(\frac{\partial^2 T}{\partial x} + \frac{\partial^2 T}{\partial y^2}) + \mu\Phi \tag{4.7}$$

The energy equation for an incompressible flow with no viscous dissipation, no compression work and without heat generation and under the assumption which is described in section 4.1 is;

$$\frac{d^2 T}{d\, y^2} = 0 \tag{4.8}$$

4.3. Boundary Conditions

The boundary conditions for momentum equation which expressed in Equation (4.5) can be written using non-slip condition as respectively;

On the left side;

$$Y = 0 \qquad U(0) = 0 \tag{4.9}$$

On the right side;

$$Y = b \qquad U(b) = 0 \tag{4.10}$$

The boundary conditions for heat transfer equation, Equation (4.8), can be written as;

On the left side;

$$Y = 0 \qquad T(0) = T_1 \tag{4.11}$$

On the right side;

$$Y = b \qquad T(b) = T_2 \tag{4.12}$$

Equation (4.5) and (4.8), using boundary conditions given in section 4.3, are solved numerically using the method described in a detail in Chapter 11. The results of these equations are given in Chapter 12.1.

CHAPTER 5

FULLY DEVELOPED MIXED CONVECTION IN A CHANNEL WITH PURE FLUID: DIMENSIONLESS GOVERNING EQUATIONS

5.1. Definition of the Problem

The same problem discussed in Chapter 4 is analyzed in this chapter again using dimensionless governing equations. Considered problem is shown in Figure 5.1. Although the studied channel and the problem are same, the governing equations which are given in Chapter 4 are nondimensionalized using dimensionless parameters and dimensionless governing equations are obtained and these equations are solved in these chapter.

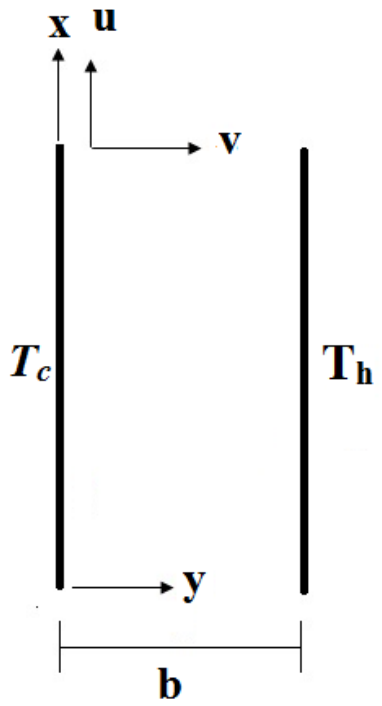

Figure 5.1. Considered problem

5.2. Governing Equations

The governing equations for laminar, mixed convection fully developed flow under the assumptions explained in Chapter 4 are continuity, momentum and heat transfer equations. Dimensional governing equations were given in previous chapter.

5.2.1. Dimensionless Continuity, Momentum and Energy Equations

The Equations (4.5) and (4.8) are needed to be solved to obtain velocity and temperature distribution in the channel. By applying Boussinesq's approximation and introducing dimensionless parameters;

$$X = \frac{x}{b}, \quad Y = \frac{y}{b}, \quad U = \frac{u}{u_0}, \quad \theta = \frac{T - T_{av}}{T_h - T_c}, \quad P = \frac{pb}{u_0 \mu}, \quad \Gamma = \frac{dP}{dX} \tag{5.1}$$

where $\mathrm{Re} = u_0 b / \nu$ is the Reynolds number, b is the gap between plates, u_o is the velocity of the inlet flow and T is the temperature. By considering, linear change of pressure in flow direction for fully developed flow; the variation of pressure along the channel can be shown by Γ which is constant. Then, Equation (4.5) and (4.8) can be written in dimensionless form respectively as;

$$\frac{d^2U}{dY^2} + \frac{Gr_{cl}}{Re}\theta - \Gamma = 0 \tag{5.2}$$

$$\frac{d^2\theta}{dY^2} = 0 \tag{5.3}$$

where $Gr_{cl} = g\beta(T_h - T_c)b^3 / \nu^2$ is the Grashof number.

5.3. Boundary Conditions

The dimensionless boundary conditions for momentum equation which expressed in Equation (5.2) can be written using non-slip condition as respectively;

On the left side;

$$Y = 0 \qquad U(0) = 0 \tag{5.4}$$

On the right side;

$$Y = 1 \qquad U(1) = 0 \tag{5.5}$$

The dimensionless boundary conditions for energy equation, Equation (5.3), can be written as;

On the left side;

$$Y = 0 \qquad \theta(0) = -0.5 \tag{5.6}$$

On the right side;

$$Y = 1 \qquad \theta(1) = 0.5 \tag{5.7}$$

5.4. Solutions of the Governing Equations

The analytical solution of Equation (5.3) with the boundary conditions expressed in Equation (5.6) and (5.7) is;

$$\theta = Y - 0.5 \tag{5.8}$$

The analytical solution of Equation (5.2) can be obtained by using the boundary conditions expressed in Equation (5.4) and (5.5);

$$U = -\frac{Gr_{cl}}{Re}\frac{Y^3}{6} + (\Gamma + \frac{Gr_{cl}}{2\,Re})\frac{Y^2}{2} - [(\frac{Gr_{cl}}{12\,Re} + \frac{\Gamma}{2})]Y \tag{5.9}$$

where Γ parameter still needs to be evaluated. Therefore, to obtain a result for Γ, one more equation is needed. The conservation of mass in the channel can be written as;

$$\int_0^1 U(Y)dY = 1 \tag{5.10}$$

Then, integration of Equation (5.10) using Equation (5.9) leads to;

$$\Gamma = -12 \tag{5.11}$$

The mean temperature which is known as;

$$\theta_m = \int_0^1 U\theta dY \tag{5.12}$$

Substituting Equation (5.8) and (5.9) into Equation (5.12) yields to;

$$\theta_m = \frac{1}{720}\frac{Gr_{cl}}{\mathrm{Re}} \tag{5.13}$$

The results of these equations are given in Chapter 12.1.2.

CHAPTER 6

FULLY DEVELOPED MIXED CONVECTION IN A CHANNEL COMPLETELY FILLED WITH POROUS MEDIA: DIMENSIONAL GOVERNING EQUATIONS

6.1. Definition of the Problem

The only difference of this chapter from Chapter 4 is that the channel is filled with saturated porous media in this case. Schematic view of the considered channel is shown in Figure 6.1. Governing equations of the problem will be investigated dimensionally.

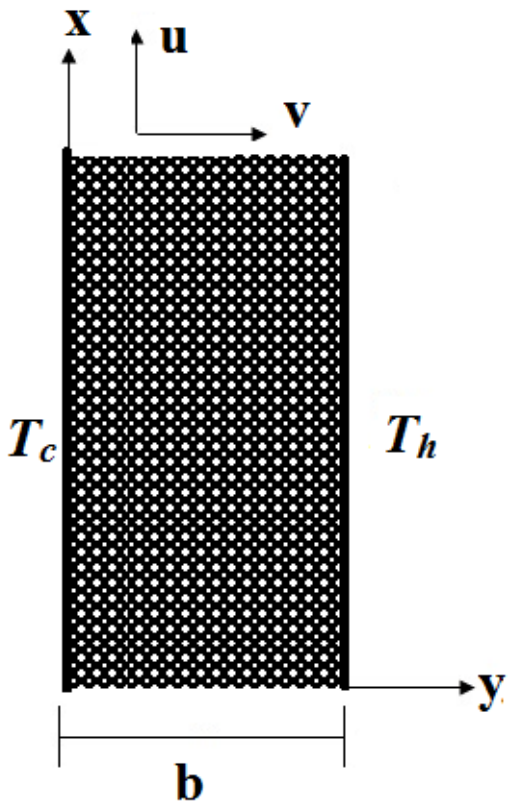

Figure 6.1. Considered problem

6.2. Governing Equations

The governing equations, continuity, fluid motion and heat transfer equations, is explained in this section.

6.2.1. Continuity Equation

The continuity equation does not get affected by adding porous media to the channel. Therefore, the continuity equation is same with the studied problem in Chapter 4.

$$\frac{d\,u}{d\,x} = 0 \tag{6.1}$$

6.2.2. Fluid Motion Equation

Brinkman-Extended-Darcy law can be used to analyze this problem as written below.

$$\mu_{eff}\frac{d^2u}{dy^2} - \frac{\mu_f}{K}u + \rho g\,\beta(T - T_{av}) - \frac{\partial p}{\partial x} = 0 \tag{6.2}$$

where μ_{eff} is effective dynamic viscosity and K is permeability.

6.2.3. Heat Transfer Equation

The energy equation for an incompressible flow with no viscous dissipation, no compression work and without heat generation and under the assumption which is described in Chapter 4;

$$\frac{d^2T}{d\,y^2} = 0 \tag{6.3}$$

6.3. Boundary Conditions

The boundary conditions for fluid motion equation which expressed in Equation (6.2) can be written using non-slip condition as respectively;

On the left side;

$$Y = 0 \qquad U(0) = 0 \tag{6.4}$$

On the right side;

$$Y = b \qquad U(b) = 0 \tag{6.5}$$

The boundary conditions for heat transfer equation, Equation (6.3), can be written as;

On the left side;

$$Y = 0 \qquad T(0) = T_c \tag{6.6}$$

On the right side;

$$Y = b \qquad T(b) = T_h \tag{6.7}$$

Equation (6.2) and (6.3), using boundary conditions given in section 6.3, are solved numerically using the method described in a detail in Chapter 11. The results of these equations are given in Chapter 12.2.

CHAPTER 7

DIMENSIONLESS STUDY ON FULLY DEVELOPED MIXED CONVECTION IN A CHANNEL COMPLETELY FILLED WITH POROUS MEDIA

7.1. Definition of the Problem

In this chapter, mixed convection between a two vertical parallel plate filled with isotropic porous media is considered. The fluid is assumed to be Newtonian and incompressible, while the flow is laminar, fully developed and steady. The channel has a rectangular cross-section with width of b. It is assumed that the plates are infinitely long in z direction, x is being vertical direction and y is perpendicular direction to x direction. It is also assumed that the flow in the channel is fully developed, unidirectional and steady. The fluid properties are assumed constant except the density in buoyancy term of the fluid motion equation. Viscous dissipation is neglected for this case. A constant temperature is applied to the walls of the channel as shown in Figure 7.1.

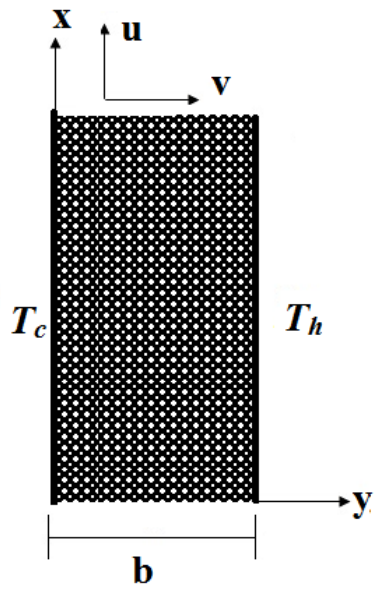

Figure 7.1. Considered problem

7.2. Governing Equations

The governing equations for laminar, mixed convection fully developed flow under the assumptions explained in the section above are continuity, fluid motion equations and energy equation. Dimensional equations are given in Chapter 6 and these equations will be made nondimensionalized in this chapter.

7.2.1. Dimensionless Continuity, Fluid Motion and Heat Transfer Equations

The Equations (6.2), (6.3) are needed to be solved to obtain velocity and temperature distribution in the channel. By applying Boussinesq's approximation and introducing dimensionless parameters;

$$X = \frac{x}{b}, \quad Y = \frac{y}{b}, \quad U = \frac{u}{u_0}, \quad \theta = \frac{T - T_{av}}{T_h - T_c}, \; P = \frac{pb}{u_o \mu_f}, \; \Gamma = \frac{dP}{dX} \tag{7.1}$$

where $\mathrm{Re} = u_0 \, b / \nu$ is the Reynolds number. By considering, linear change of pressure in flow direction for fully developed flow; the variation of pressure along channel can be shown by Γ which is constant. Then, Equation (6.2), (6.3) can be written in dimensionless form as;

$$\frac{d^2U}{dY^2} - \frac{M}{Da}U + M\frac{Gr_p}{Re}\theta - M\Gamma = 0 \tag{7.2}$$

$$\frac{d^2\theta}{dY^2} = 0 \tag{7.3}$$

where $Gr_p = \rho g \, \beta K (T_h - T_c) b \; / \nu^2$ is the Darcy-modified Grashof number.

7.3. Boundary Conditions

The dimensionless boundary conditions for fluid motion equation which expressed in Equation (7.2) can be written using non-slip condition as respectively;

On the left side;

$$Y = 0 \qquad U(0) = 0 \tag{7.4}$$

On the right side;

$$Y = 1 \qquad U(1) = 0 \tag{7.5}$$

The dimensionless boundary conditions for energy equation, Equation (7.3), can be written as;

On the left side;

$$Y = 0 \qquad \theta(0) = -0.5 \tag{7.6}$$

On the right side;

$$Y = 1 \qquad \theta(1) = 0.5 \tag{7.7}$$

7.4. Solutions of the Governing Equations

The analytical solution of Equation (7.3) with the boundary conditions expressed in Equation (7.6) and (7.7) is;

$$\theta = Y - 0.5 \tag{7.8}$$

The analytical solution of Equation (7.2) can be obtained by using the boundary conditions expressed in Equation (7.4) and (7.5);

$$U = C_1 Y + C_2 \, sinh(S(Y-1)) + C_3 \, sinh(SY) + C_4 \tag{7.9}$$

where C_1, C_2, C_3 and C_4 are constants given in Appendix, and $S = \sqrt{M / Da}$. Γ parameter still needs to be evaluated. Therefore, to obtain a result for Γ, one more equation is needed. The conservation of mass in the channel can be written as;

$$\int_0^1 U(Y) dY = 1 \tag{7.10}$$

Then, integration of Equation (7.10) using Equation (7.9) leads to;

$$\Gamma = \frac{\sqrt{M}}{Da(-\sqrt{M} + 2\sqrt{Da}\tanh(\frac{S}{2})} \tag{7.11}$$

The results of these equations are given in Chapter 12.2.2.

CHAPTER 8

FULLY DEVELOPED MIXED CONVECTION IN A CHANNEL PARTIALLY FILLED WITH POROUS MEDIA: DIMENSIONAL GOVERNING EQUATIONS

8.1. Definition of the Problem

The only difference between this chapter and the explained problem in Chapter 6 is that the channel is partially filled with porous media. Considered problem is shown in Figure 8.1 schematically.

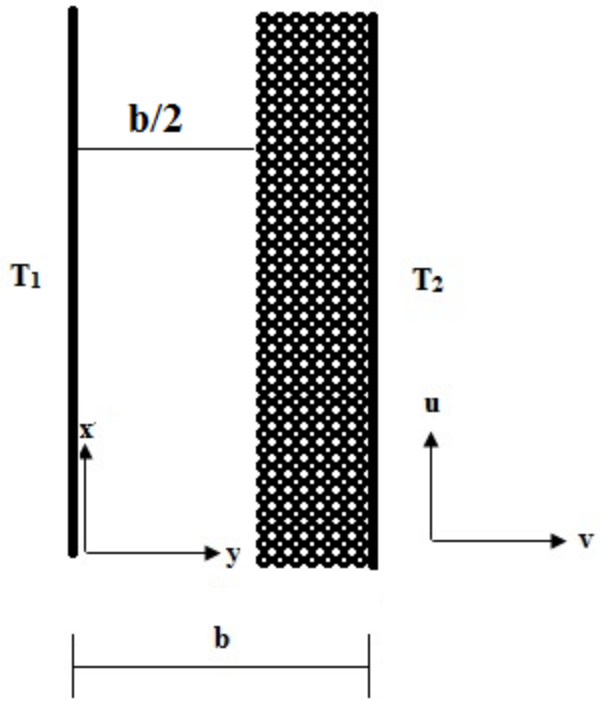

Figure 8.1. Considered problem

8.2. Governing Equations

The governing equations for laminar, mixed convection fully developed flow under the assumptions explained in Chapter 4 and 6 are continuity, fluid motion and heat transfer equations. Brinkman-Extended Darcy law is used to examine porous section. Dimensional governing equations were given in Chapter 4 and Chapter 6.

8.3. Boundary Conditions

In this section, boundary conditions for pure fluid part and saturated porous section is given separately. The dimensional fluid motion equation (Equation 4.5) boundary conditions for pure fluid part are;

On the left side;

$$Y = 0 \qquad U(0) = 0 \tag{8.1}$$

On the right side;

$$Y = b/2 \qquad U(b/2) = U_i \tag{8.2}$$

The dimensional boundary conditions for energy equation, Equation (4.8), can be written as;

On the left side;

$$Y = 0 \qquad T(0) = T_1 \tag{8.3}$$

On the right side;

$$Y = b/2 \qquad T(b/2) = T_i \tag{8.4}$$

The dimensional fluid motion equation (Equation 6.2) boundary conditions for saturated porous part are;

On the left side;

$$Y = b/2 \qquad U(b/2) = U_i \tag{8.5}$$

On the right side;

$$Y = b \qquad U(b) = 0 \tag{8.6}$$

The dimensional boundary conditions for energy equation, Equation (6.3), can be written as;

On the left side;

$$Y = b/2 \qquad T(b/2) = T_i \tag{8.7}$$

On the right side;

$$Y = b \qquad T(b) = T_2 \tag{8.8}$$

CHAPTER 9

FULLY DEVELOPED MIXED CONVECTION IN A CHANNEL PARTIALLY FILLED WITH POROUS MEDIA: DIMENSIONLESS GOVERNING EQUATIONS

9.1. Definition of the Problem

Fully developed mixed convection in a channel partially filled with porous media is investigated in this chapter dimensionless. The assumptions which are given in Chapter 4 are also valid for this chapter.

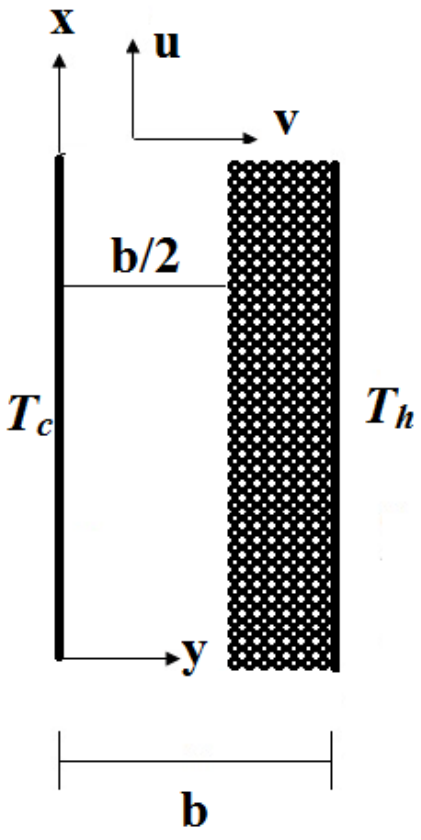

Figure 9.1. Considered problem

9.2. Governing Equations

The governing equations for laminar, mixed convection fully developed flow under the assumptions explained in Chapter 4 and 8 are continuity, fluid motion and heat transfer equations. Dimensional governing equations were given in previous chapter. These governing equations are non-dimensionalized in this chapter.

9.2.1. Dimensionless Continuity, Fluid Motion and Energy Equations

The Equations (4.5) and (4.8) for clear fluid layer and (6.2) and (6.3) for porous layer are needed to be solved to obtain velocity and temperature distribution in the channel. By applying Boussinesq's approximation and introducing dimensionless parameters given in Equation (5.1), dimensionless momentum and heat transfer equations can be written as in Equation (5.2) and (5.3) for pure fluid part. Using the same dimensionless parameters dimensionless governing equations for saturated porous part can be found as in Equation (7.2) and (7.3).

9.3. Boundary Conditions

In this section, boundary conditions for pure fluid part and saturated porous section is given separately. The dimensionless momentum equation (Equation 5.2) boundary conditions for pure fluid part are;

On the left side;

$$Y = 0 \qquad U(0) = 0 \tag{9.1}$$

On the right side;

$$Y = 0.5 \qquad U(0.5) = U_i \tag{9.2}$$

The dimensionless boundary conditions for energy equation, Equation (5.3), can be written as;

On the left side;

$$Y = 0 \qquad \theta(0) = -0.5 \tag{9.3}$$

On the right side;

$$Y = 0.5 \qquad \theta(0.5) = \theta_i \tag{9.4}$$

The dimensionless fluid motion equation (Equation 6.2) boundary conditions for saturated porous part are;

On the left side;

$$Y = 0.5 \qquad U(0.5) = U_i \tag{9.5}$$

On the right side;

$$Y = 1 \qquad U(1) = 0 \tag{9.6}$$

The dimensionless boundary conditions for energy equation, Equation (6.3), can be written as;

On the left side;

$$Y = 0.5 \qquad \theta(0.5) = \theta_i \tag{9.7}$$

On the right side;

$$Y = 1 \qquad \theta(1) = 0.5 \tag{9.8}$$

9.4. Solutions of the Governing Equations

The dimensional governing equations are made dimensionless using the dimensionless parameters explained in Equation (7.1). The analytical solutions of the heat transfer and fluid motion equations for the left half part with clear fluid section using the boundary conditions given by Equation. (9.3) and (9.4) are obtained as follows;

$$\theta_c = (2\theta_i + 1)Y - 1/2 \tag{9.9}$$

$$U_c = C_5 Y + 2U_i Y + C_6 Y^2 - C_7 Y^3 + \Gamma(-\frac{Y}{4} + \frac{Y^2}{2}) \tag{9.10}$$

where C_5, C_6 and C_7 are constants and their values are presented in Appendix. Similarly, the temperature and velocity profiles equation for fluid saturated porous region can be obtained as:

$$\theta_p = 2\theta_i - Y(2\theta_i - 1) - 1/2 \tag{9.11}$$

$$U_p = C_8 \sinh(S - SY) - C_9 \sinh(S(Y - 1/2)) - C_{10} Y + C_{11} \tag{9.12}$$

where C_8, C_9 and C_{10} and C_{11} are constants and their values are given in Appendix. U_p and U_c show velocity of fluid in clear fluid and porous regions. By using condition of continuous shear stress and heat flux at the interface, U_i and θ_i which are interface velocity and temperature can be found as:

$$U_i = \frac{C_{12}(\sinh(S/2))^2 + C_{13}\sinh(S/2) - C_{14}(\cosh(S) - 1)}{C_{15}\sinh(S) + C_{16}(\sinh(S/2))^2 + C_{17}\sinh(S/2)} \tag{9.13}$$

$$\theta_i = -\frac{K - 1}{2(K + 1)} \tag{9.14}$$

where K is thermal conductivity ratio of the fluid to effective conductivity ratio of the porous medium and Γ parameter still is needed to be evaluated. The conservation of mass in the channel can be expressed as:

$$\int_0^{0.5} U_c(Y)dY + \int_{0.5}^{1} U_p(Y)dY = 1 \tag{9.15}$$

The integration of Equation (9.15) yields Γ value as:

$$\Gamma = \frac{C_{18}(\sinh(S/2))^2 + C_{19}\sinh(S/2) + C_{20}(\cosh(S/2) - 6MS\frac{Gr_p}{\mathrm{Re}}}{C_{21}\cosh(S/2) + C_{22}(\sinh(S/2))^2 + C_{23}\sinh(s/2) - 12MS} \tag{9.16}$$

where C_{18}, C_{19}, C_{20}, C_{21}, C_{22} and C_{23} are constants and they are defined in Appendix.

The results of these equations are given in Chapter 12.3.2.

CHAPTER 10

HEATFUNCTIONS

Heatfunction and heatlines are used to visualize and explain the path of the flow of energy. For a two-dimensional, incompressible and steady flow with neglecting viscous dissipation, heat flux vector in x and y directions respectively can be expressed as;

$$J_x = \rho u C_p (T - T_{ref}) - k \frac{\partial T}{\partial x} \tag{10.1}$$

$$J_y = \rho v C_p (T - T_{ref}) - k \frac{\partial T}{\partial y} \tag{10.2}$$

where T_{ref} is reference temperature. In Cartesian coordinates, heat flux vector can be written as;

$$J = J_x \mathbf{i} + J_y \mathbf{j} \tag{10.3}$$

For fully developed flow;

$$v = 0, \qquad \frac{\partial T}{\partial x} = 0 \tag{10.4}$$

Therefore, for fully developed flow and by assuming h as a continuous scalar function, the heatfunction can be written as;

$$J_x = \rho u C_p (T - T_{ref}) - k \frac{\partial T}{\partial x} = \frac{\partial h}{\partial y} \tag{10.5}$$

$$J_y = \rho v C_p (T - T_{ref}) - k \frac{\partial T}{\partial y} = -\frac{\partial h}{\partial x} \tag{10.6}$$

The Equation (10.5) and (10.6) can be written in dimensionless form using dimensionless parameters in Equation (5.1) as;

$$\frac{\partial H}{\partial Y} = PeU(\theta + 1/2) \tag{10.7}$$

$$\frac{\partial H}{\partial X} = \frac{\partial \theta}{\partial Y} \tag{10.8}$$

where T_{ref} is accepted as T_c and H is dimensionless heatfunction:

$$H = \frac{h}{k(T_h - T_c)} \tag{10.9}$$

and Peclet number which is a dimensionless number and defined as the ratio of advection of a physical quantity by the flow to the rate of diffusion of the same quantity can be expressed as:

$$Pe = \frac{\rho c_p u_0 b}{k} \tag{10.10}$$

Thermal conductivity plays an important role on definition of dimensionless heatfunction. There is no doubt that for the channel with completely clear fluid, k is the thermal conductivity of fluid (k_f) and consequently $H_f = h/(k_f (T_h - T_c))$ and $Pe_f = \rho c_p u b / k_f$. Another important point in determination of heatfunction is the reference value for heatfunction. H_f and Pe_f are dimensionless heatfunction and Peclet number for the clear fluid channel. In this study, the value of heat function at the origin is assumed zero, $H_f(0,0) = 0$. The following equations can be written based on taking integral from Equation (10.7) and (10.8):

$$H_f(X,Y) = \int PeU(\theta + 1/2)dY + C_{24}(X) \tag{10.11}$$

$$H_f(X,Y) = X + C_{25}(Y) \tag{10.12}$$

The heatfunction should be valid for the whole of domain. The value of $C_{25}(0)$ can be found by applying Equation (10.12) for the origin:

$$H_f(0,0) = C_{25}(0) = 0 \tag{10.13}$$

The Eq (10.11) and (10.12) are also valid for Y = 0 surface, then

$$H_f(X,0) = C_{24}(X) + C_{26} \tag{10.14}$$

$$H_f(X,0) = X + C_{25}(0) \tag{10.15}$$

From the above equations, $C_{24}(X)$ can be found as:

$$C_{24}(X) = X + C_{26} \tag{10.16}$$

Therefore, the heatfunction can be expressed as:

$$H_f(X,Y) = \int PeU(\theta + 1/2)dY + X + C_{26} \tag{10.17}$$

Therefore, heatfunction equation for channel with fully clear fluid can be obtained as:

$$H_f(X,Y) = X + Pe(-\frac{Gr_c}{Re}\frac{Y^5}{30} + (\frac{\Gamma}{8} + \frac{Gr_c}{16Re})Y^4 + (-\frac{\Gamma}{6} - \frac{Gr_c}{36Re})Y^3) \tag{10.18}$$

The value of C_{26} and integral constant are zero since $H(0,0) = 0$.

The Equations (10.7) and (10.8) are valid for dimensionless heatfunction in a channel with completely porous medium. However, the effective thermal conductivity of porous medium should be used for the definition of dimensionless heatfunction and Peclet numbers and consequently, $H_p = h/(k_{eff}(T_h - T_c))$ and $Pe_p = \rho c_p u b / k_{eff}$, where k_{eff} is effective thermal conductivity and can be described as $k_{eff} = \varepsilon k_f + (1-\varepsilon)k_s$. Similar to the procedure performed to obtain Equation (10.18), the heatfunction equation for the channel filled with fluid saturated porous medium can be obtained as:

$$\begin{aligned} H_P(X,Y) = X + Pe(&\frac{C_1}{3}Y^3 - \frac{1}{S^2}(C_3 sinh(SY) - S(C_2 Y cosh(S(Y-1)) \\ &+ C_3 Y cosh(SY)) + C_2 sinh(S(Y-1))) + C_4\frac{Y^2}{2} + C_2 sinh(S)) \end{aligned} \tag{10.19}$$

where C_1, C_2, C_3 *and* C_4 are constants and the related equations are given in Appendix.

Similarly, for the channel with partially filled porous medium, the dimensionless heatfunction for the clear fluid region can be found from the following equation:

$$\frac{\partial H_f}{\partial Y} = Pe_f U(\theta + 1/2) \tag{10.20}$$

$$\frac{\partial H_f}{\partial X} = \frac{\partial \theta}{\partial Y} = (2\theta_i + 1) \tag{10.21}$$

Heatfunction differential equation for the porous medium region can also be found from the following equations:

$$\frac{\partial H_p}{\partial Y} = Pe_p U(\theta + 1/2) \tag{10.22}$$

$$\frac{\partial H_p}{\partial X} = \frac{\partial \theta}{\partial Y} = (1 - 2\theta_i) \tag{10.23}$$

The comparison between the definitions of dimensionless heatfunction for clear fluid and porous medium filled regions (i.e., $H_f = h/(k_f (T_h - T_c))$ and $H_p = h/(k_{eff} (T_h - T_c))$) show that the values of H_f and H_p are not the same on the solid–fluid interface and a discontinuity exits. A point on the interface has two dimensionless heatfunction values due to different definitions of H_f and H_p. Finding a relation between H_f and H_p may be a solution for this difficulty.

$$H_p = \frac{h}{k_f (T_h - T_c)} \frac{1}{K} = H_f K \tag{10.24}$$

By substituting Equation (10.24) into Equations (10.22) and (10.23), the following equations can be obtained for the porous medium region in the channel.

$$\frac{\partial H_f}{\partial Y} = Pe_f U(\theta + 1/2) \tag{10.25}$$

$$\frac{\partial H_f}{\partial X} = \frac{1}{K}\frac{\partial \theta}{\partial Y} = \frac{1}{K}(1 - 2\theta_i) \tag{10.26}$$

As seen, Equations (10.25) and (10.26), the heatfunction for porous region is defined based on the fluid thermal conductivity. By the other words, the fluid thermal conductivity is used to define dimensionless heatfunction in the entire channel, and no discontinuity of dimensionless heatfunction will be faced at the interface. Similar method, used to find Equation (10.18), can be employed to determine dimensionless heatfunction for the clear and porous medium regions. Dimensionless heatfunction for the left half of the channel can be obtained as:

$$H_f = (2\theta_i + 1)X + \frac{((2\theta_i + 1)PeY^3(40C_5 - 10\Gamma + 80U_i + 30C_6Y + 15\Gamma Y - 24C_7Y^2)}{120} \quad (10.27)$$

The dimensionless heatfunction for right half of the channel region is:

$$\begin{aligned} H_f = {} & (1-2\theta_i)X/K + C_{11}2\theta_i PeY - C_{27}Y^2 + C_{28}Y^3 - C_{29}\sinh(S(1-Y)) \\ & + C_{30}\sinh(S(Y-1/2)) - C_{31}\cosh(S(1-Y)) - C_{32}\cosh(S(Y-1/2)) \\ & - C_{33}Y\cosh(S(1-Y)) - C_{34}Y\cosh(S(Y-1/2)) + C_{35} - C_{36} \end{aligned} \quad (10.28)$$

CHAPTER 11

NUMERICAL APPROACH FOR THE SOLUTION OF GOVERNING EQUATIONS

In this chapter, the numerical solution of governing equations by using finite difference method is explained. 101 nodes in Y or X directions are used in solving all governing equations. The employed nodal equations are given for each studied cases in following subsections.

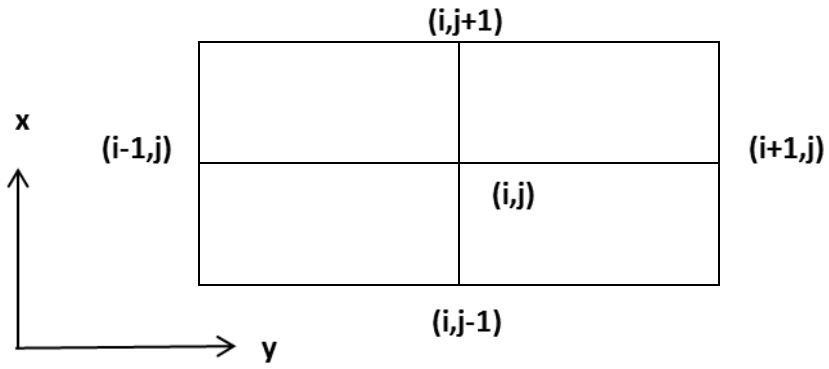

Figure 11.1 Node system used to solve the equations

In Figure 11.1, nodal system followed to obtained numerical solution can be seen. Distance between two cells is Δy. Thus, central difference in y direction is $\frac{\partial F}{\partial y} = \frac{F(i+1, j) - F(i-1, j)}{2\Delta y}$ while central difference in x direction is $\frac{\partial F}{\partial x} = \frac{F(i, j+1) - F(i, j-1)}{2\Delta x}$.

11.1. Nodal Equations for Pure Fluid Channel

Nodal equations of governing equations for pure fluid channel, which are given in Chapter 4, can be written as follows:

For momentum equation, Equation (4.5):

$$u(i) = \mu \frac{u(i+1) + u(i-1)}{2\Delta y^2} - \frac{A}{2} + \rho g \beta (T(i) - T_{av}) \tag{11.1}$$

where A stands for Γ .For heat transfer equation, Equation (4.8):

$$T(i) = \frac{T(i+1) + T(i-1)}{\Delta y^2} \tag{11.2}$$

11.2. Nodal Equations for Fully Porous Channel

For fluid motion equation, Equation (6.2):

$$u(i) = \frac{\mu_{eff}}{B} \frac{u(i+1) + u(i-1)}{\Delta y^2} - \frac{A}{B} + \frac{\rho g \beta (T(i) - T_{av})}{B} \tag{11.3}$$

where A stands for Γ and $B = \frac{2}{\Delta y^2} + \frac{\mu_f}{K}$ (11.4)

For heat transfer equation, Equation (6.3):

$$T(i) = \frac{T(i+1) + T(i-1)}{\Delta y^2} \tag{11.5}$$

11.3. Nodal Equations for Partially Porous Channel

Momentum equation for pure fluid section:

$$u(i) = \mu \frac{u(i+1) + u(i-1)}{2\Delta y^2} - \frac{A}{2} + \rho g \beta (T(i) - T_{av}) \tag{11.6}$$

Fluid motion equation for porous section:

For fluid motion equation, Equation (6.2):

$$u(i) = \frac{\mu_{eff}}{B} \frac{u(i+1) + u(i-1)}{\Delta y^2} - \frac{A}{B} + \frac{\rho g \beta (T(i) - T_{av})}{B} \tag{11.7}$$

where A stands for Γ and $B = \frac{2}{\Delta y^2} + \frac{\mu_f}{K}$

11.4. Elliptic PDEs

In this section, an elliptic partial differential equation for dimensionless heatfunction is derived and numerical method to solve these PDEs is explained.

Taking derivatives with respect to y and x from Equations (10.5) and (10.6) leads to:

$$\rho Cp \frac{\partial}{\partial y}(u(T - T_{ref})) = \frac{\partial^2 h}{\partial y^2} \tag{11.8}$$

$$-k \frac{\partial^2 T}{\partial x \partial y} = -\frac{\partial^2 h}{\partial x^2} \tag{11.9}$$

For mixed convection fully developed flow, $\frac{\partial}{\partial y}(\frac{\partial T}{\partial x}) = 0$. The summation of Equation (11.8) and (11.9) yields partial differential heatfunction equation:

$$\frac{\partial^2 h}{\partial x^2} + \frac{\partial^2 h}{\partial y^2} = \rho Cp \frac{\partial}{\partial y}(u(T - T_{ref})) \tag{11.10}$$

The above heatfunction equation, which is an elliptical partial differential equation, can be written in dimensionless form.

$$\frac{\partial^2 H}{\partial X^2} + \frac{\partial^2 H}{\partial Y^2} = Pe \frac{\partial}{\partial y}(U(\theta + \frac{1}{2})) \tag{11.11}$$

where T_{ref} is accepted as T_c. The solution of Equation (11.11) yields the distribution of heatfunction in the channel. The boundary conditions for heatfunction equation can be written by using Equations (10.7) and (10.8):

$$\text{For } Y = 0 \; H(X,0) = \int_{X=0}^{X} \left.\frac{\partial \theta}{\partial Y}\right|_{Y=0} dX \tag{11.12}$$

$$\text{For } Y = 1 \; H(X,1) = \int_{X=0}^{X} \left.\frac{\partial \theta}{\partial Y}\right|_{Y=1} dX \tag{11.13}$$

$$\text{For } X = 0 \; H(0,Y) = \int_{Y=0}^{Y} PeU(\theta + 1/2) dY \tag{11.14}$$

$$\text{For } X = X_0 \; H(X_0,Y) = \int_{Y=0}^{Y} PeU(\theta + 1/2)\, dY \tag{11.15}$$

where X_0 is the ratio of b/L. The above differential equation is valid for completely clear fluid channel or completely porous medium filled channel. For the channel partially

filled with porous medium, θ, H and Pe are replaced with θ_c H_f, Pe_f for the left half of the channel, and the same parameters are replaced with θ_p, H_p and Pe_p for the right half of the channel. Then, KH_f can be written instead of H_p. The value of H_f at the interface can be calculated by the following relation:

$$\text{For } Y = 0.5 \; H(X, 0.5) = \int_{X=0}^{X} \left. \frac{\partial \theta_f}{\partial Y} \right|_{Y=0.5} dX \tag{11.16}$$

The Equation(11.11) can be solved numerically by using the following nodal equation:

$$H(i,j) = \frac{1}{\frac{2}{\Delta x^2} + \frac{2}{\Delta y^2}} \left(\frac{H(i,j+1) + H(i,j-1)}{\Delta x^2} + \frac{H(i+1,j) + H(i-1,j)}{\Delta y^2} \right.$$
$$\left. - Pe \left(\frac{\theta(i+1,j) U(i+1,j) - \theta(i-1,j) U(i-1,j)}{2\Delta y} + \frac{U(i+1,j) + U(i-1,j)}{4\Delta y} \right) \right) \tag{11.17}$$

where H is dimensionless heatfunction, θ for each case is given in Chapter 5, 7 and 9. Boundary conditions are given in Equation (11.12), (11.13), (11.14), (11.15) and (11.16) for elliptic PDE. Following same central difference method, these boundary conditions can be also evaluated numerically.

CHAPTER 12

RESULTS AND DISCUSSIONS

Three different channels are studied in this thesis. The first channel is filled with completely pure fluid; the second one is completely filled with fluid saturated porous medium. A porous layer exists in the half of the third channel while another half is filled with pure fluid. Obtained results of the studied problems explained in previous chapters are given in this chapter. Results are explained for each chapter in separate subheadings and discussions are made. First, the results for pure fluid channel are which is investigated in Chapter 4 and 5, discussed dimensionally in section 12.1.1 and dimensionless in section 12.1.2. Completely filled porous channel is analyzed dimensional and dimensionless in section 12.2.1 and 12.2.2 separately. Then, partially filled porous channel is discussed in section 12.3.1 and 12.3.2. Finally, heatfunctions are discussed in section 12.4.

12.1. Obtained Results for Fully Clear Channel

Discussions for fully clear channel are studied in this subsection.

12.1.1. Dimensional Results

The momentum and heat transfer equations are solved numerically. The numerical solution procedure is explained in Chapter 10. The considered channel is shown in Figure 4.1. T_2 temperature is kept constant at 100 ^{0}C degree and T_1 is changed from 0 to 80 ^{0}C. Velocity is also taken as 0.2 m/s. The gap is taken 25 and 50mm. Using $Gr_c = g\beta(T_2 - T_1)b^3/\nu^2$, Gr_c/Re values are calculated for four different T_1 temperatures and it is given in Table 12.1. As it can be seen from Table 12.1, a decrease of temperature difference between plates results in decrease of Gr_c/Re ratio which means buoyancy effects lose their effectiveness with decrease of temperature difference.

Table 12.1.Gr_c/Re values for different cold temperatures while the gap is 25 mm

T_c [^{0}C]	T_h [^{0}C]	Velocity [m/s]	Gr_c/Re
0	100	0.2	530
40	100	0.2	270
60	100	0.2	166
80	100	0.2	77
99	100	0.2	3

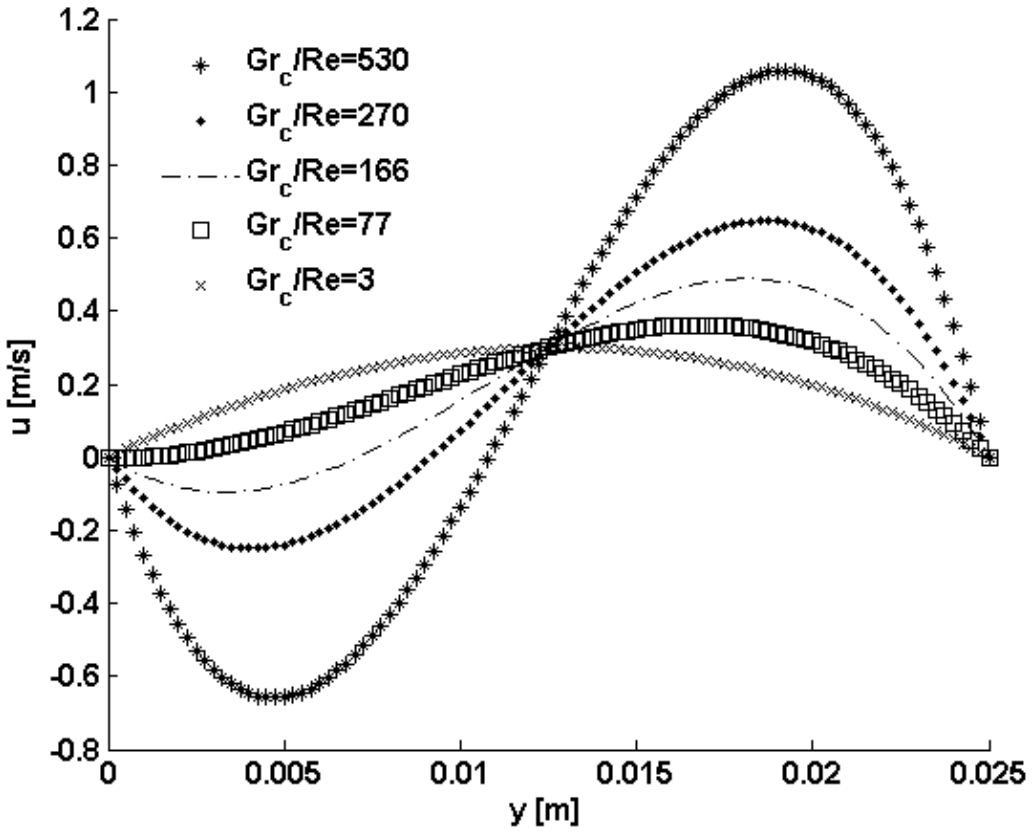

Figure 12.1. Dimensional velocity profiles for different Gr_c/Re values in a vertical channel while the gap between plates is 25 mm

Figure 12.1 shows the velocity profiles for different values of T_c temperature in a vertical channel where the gap between plates, b, is 25 mm. T_h value is kept at 100 ^{0}C. As it can be seen from the figure, with decreasing temperature difference which causes decreasing in Gr_c/Re ratio, the buoyancy effects decreases. Therefore, forced convection becomes dominant and a parabolic velocity profile occurs. However, the increase of temperature difference (e.g. ΔT = 100 ^{0}C) causes the increase of buoyancy effect and

consequently Gr_c/Re ratio increases. That is why flow reversal is seen near cold plate due to fixed flow rate.

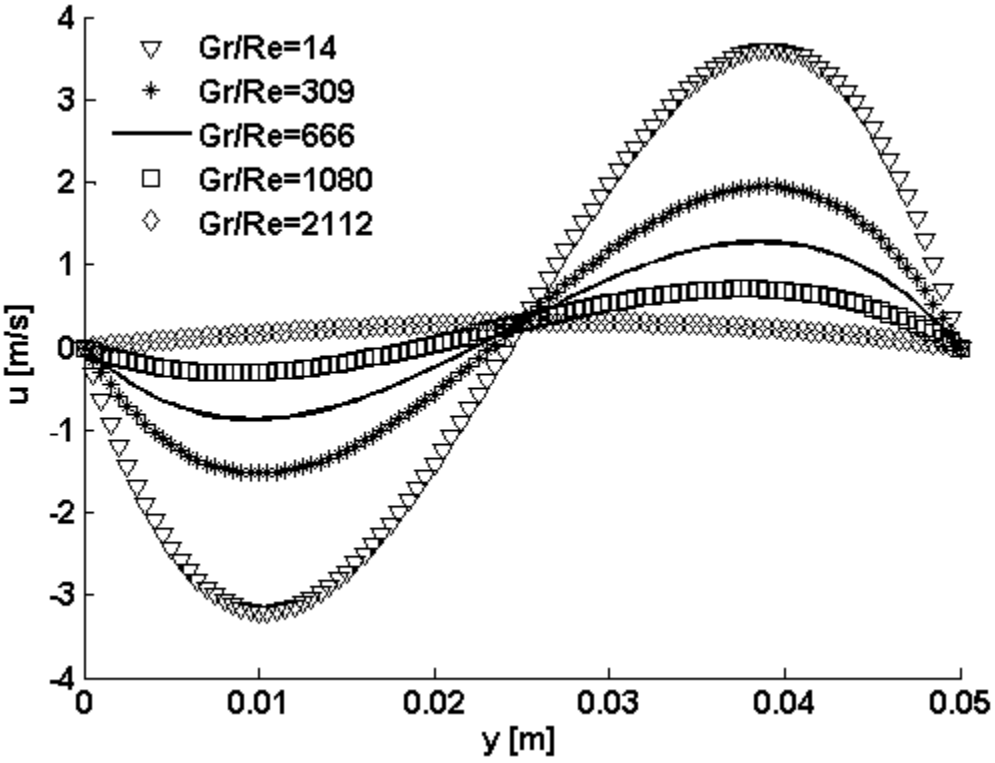

Figure 12.2. Dimensional velocity profiles for different Gr_c/Re values in a vertical channel while the gap between plates is 50 mm

Table 12.2 Gr_c/Re values for different cold temperatures while the gap is 50 mm

T_c [^{0}C]	T_h [^{0}C]	Velocity [m/s]	Gr/Re
0	100	0.2	2112
40	100	0.2	1080
60	100	0.2	666
80	100	0.2	309
99	100	0.2	14

Figure 12.2 also shows velocity profile in the channel for different values of Gr_c/Re. However, the gap between plates, b, is taken 50 mm this time. T_1 temperature is changed from 0 to 99, as seen on Table 12.2 while T_2 value is kept constant. The variation of velocity profile with Gr_c/Re is similar with Figure 12.1. By decreasing of temperature difference between two walls, the buoyancy effect decreases, forced convection become dominant and a parabolic velocity profile occurs. However with

increasing of temperature difference reverse flow occurs. Although variation of velocity profile similar with Figure 12.1, the maximum velocity values are higher than Figure 12.1 as a result of high Gr_c/Re numbers due to increasing gap, 50 mm, between plates because using the definition of Gr_c dimensionless number, we can see that increasing gap between plates means increasing Gr_c number and increasing Gr_c number means more effective buoyancy forces. Thus, with increasing gap between plates, buoyancy forces are getting stronger and therefore, velocity near hot plate increases due to increasing Gr_c number.

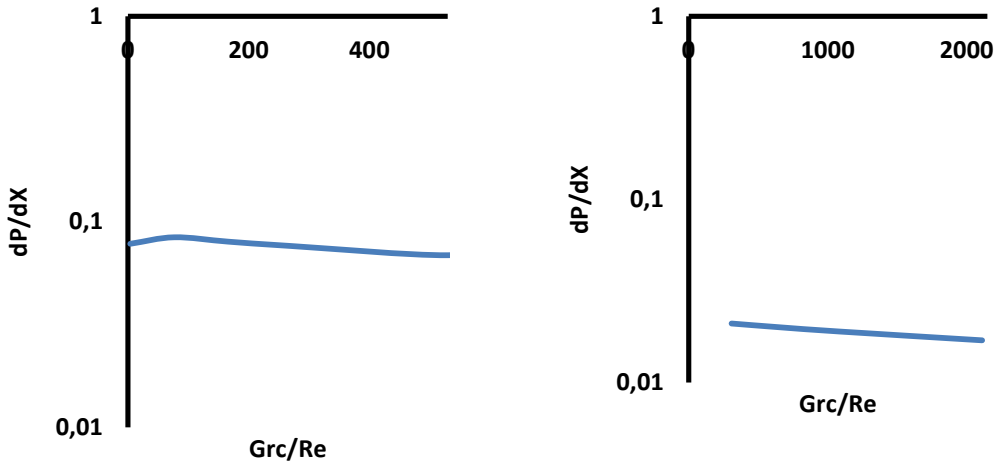

(a) (b)

Figure 12.3. Change of pressure gradient with Gr_c/Re numbers for pure fluid channel a) The gap is 25 mm b) The gap is 50 mm

Figure 12.3 shows pressure gradient along the channel for different values of Gr_c/Re and the gap between plates. The gap is taken as 25 and 50 mm. As seen from Figure 12.3(a), the pressure gradient along the channel is nearly the same with a change of Gr_c/Re value. However, the pressure gradient increases along the channel with a change of the gap between plates, *b*. The pressure gradient values in a channel with a gap of 25 mm are approximately ten times greater than the gradient of the channel with gap of 50 mm.

12.1.2. Dimensionless Results

In this subsection, the results of the dimensionless study defined in Chapter 5 are given and discussions are made. The considered channel is given in Figure 5.1. The

flow in the channel is thermally and hydrodynamically laminar. For the presented results M = 1, the value of Gr/Re number is changed from 0 to 750. The Equations (5.2) and (5.3) which are motion equation and heat transfer equation described in detail in Chapter 5 are considered and the solution of these equations which are Equation (5.8) and (5.9) are used to obtain results.

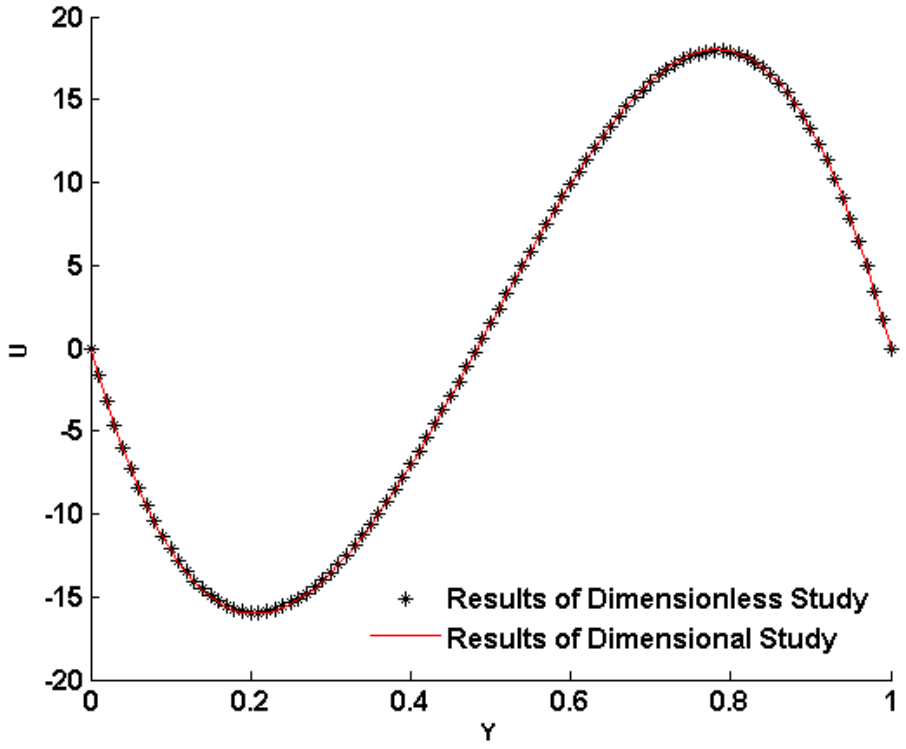

Figure 12.4. Comparison of dimensional and dimensionless study for pure fluid channel, $Gr_c/Re = 14$

Figure 12.4 shows the comparison between the dimensional and dimensionless study. For $Gr_c/Re = 14$, the dimensional results represented in section 12.1.1 by Figure 12.2 are made dimensionless by using parameters defined by Equation (5.1). Then, the dimensionless form of Figure 12.2 for Gr / Re = 14 is presented in Figure 12.4. Moreover, the velocity expressions represented by Equation (4.5) and analytically found for dimensionless differential equation of motion equation (Equation 5.9) are used and dimensionless velocity profile is plotted for Gr / Re = 14 in the same figure. As seen, there is a good agreement between the analytical values and numerical values based on the dimensional results.

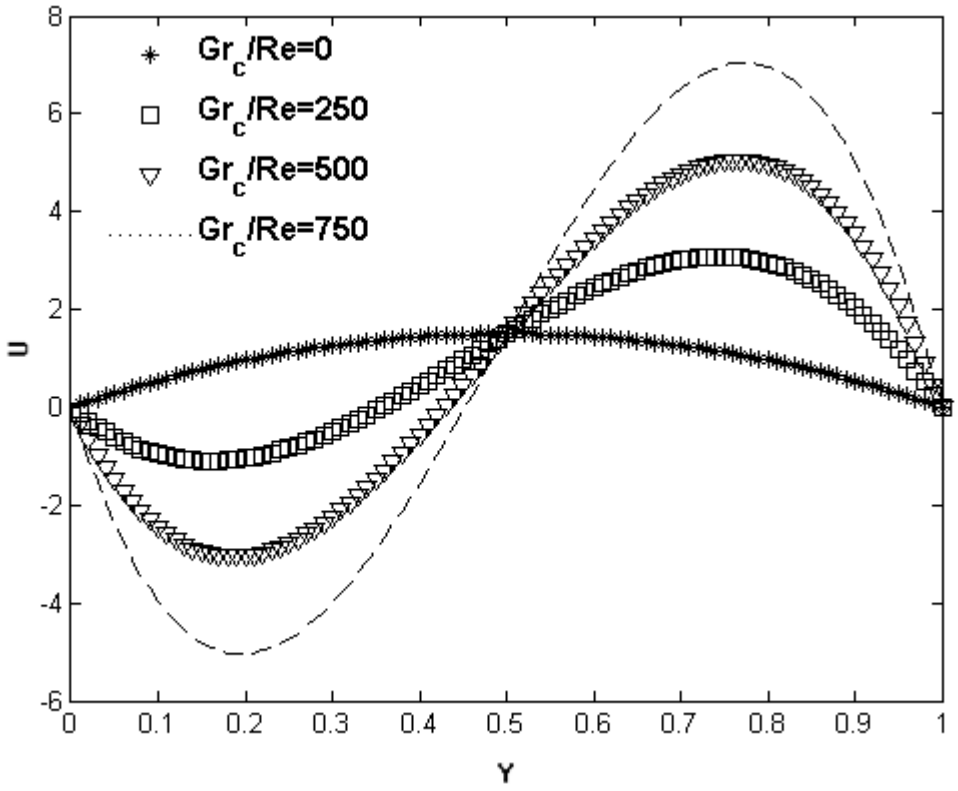

Figure 12.5. The change of velocity profile with Gr_c/Re numbers for pure fluid channel, dimensionless study

The change of dimensionless velocity profile with Gr_c/Re number is seen from Figure 12.5. The velocity profile is parabolic when Gr_c/Re number is zero where the buoyancy force does not exist. When the buoyancy effect is not effective, the force convection is the only dominant heat transfer mechanism, and a parabolic velocity profile is observed for Gr_c/Re numbers. However, with increasing Gr_c/Re number, the temperature difference between the parallel plate increases and the velocity of flow near hot plate becomes higher than the flow near cold plate. Thus, a flow reversal is seen due to the fixed flow rate.

12.2. Obtained Results for Channel Completely Filled with Porous Medium

As it is discussed in Chapter 6 and 7, the same channel studied in Chapter 4 and 5 is studied again but this time the studied channel is filled with porous media. The governing equations are continuity, Brinkman-Darcy fluid motion equation and heat transfer equations. These equations are solved for a case (i.e. $T_c = 0C \;\; T_h = 800C$) and

then made dimensionless using the dimensionless parameters, as it is explained in Chapter 5. Then, a comparison between dimensional and dimensionless study and discussions are made in following subsections.

12.2.1. Dimensional Study

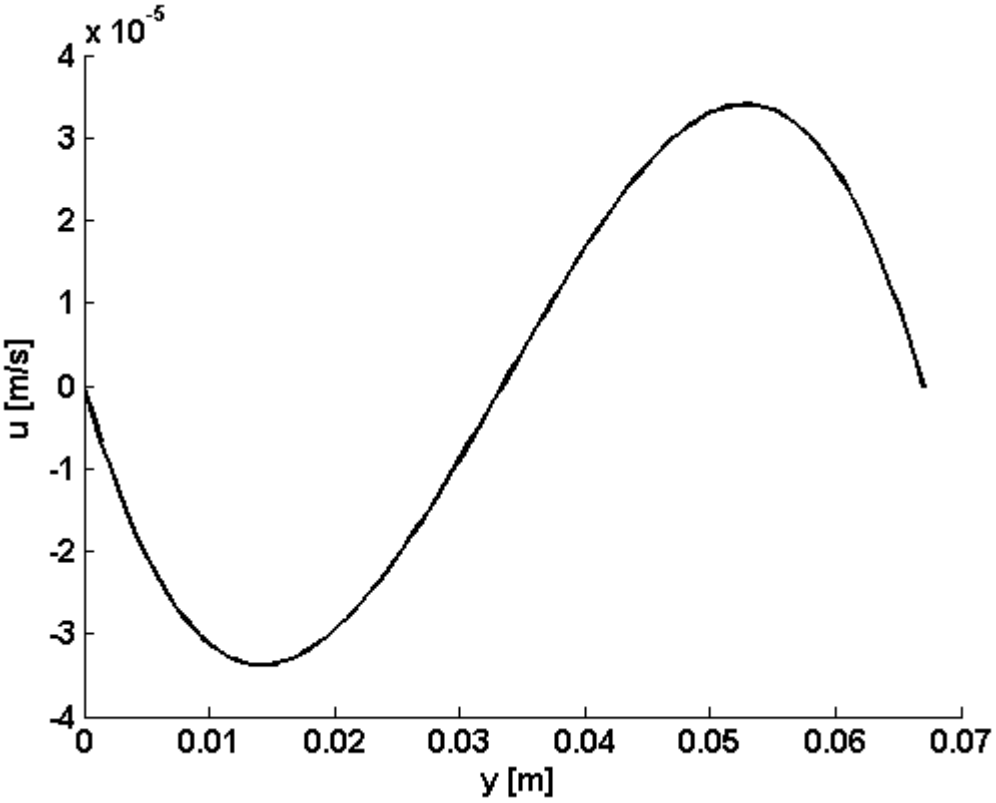

Figure 12.6. Dimensional study for fully filled porous channel, b=67 mm, K=0.40 (m^2)

Figure 12.6 shows velocity profile of the dimensional study for fully porous channel. The gap between plates is taken 67 mm. The temperature of the cold plate is 0 ^oC while the hot plate is kept at 800 ^oC. 2.5 mm square bars are placed in the channel with the 4.2 mm distance. Using the Equation (3.3), the permeability, K, is calculated as 0.40 and Darcy number is calculated as $2.49x10^{-5}$. As a result of high temperature differences which mean strong buoyancy forces, flow reversal is seen near the cold plate due to fixed flow rate.

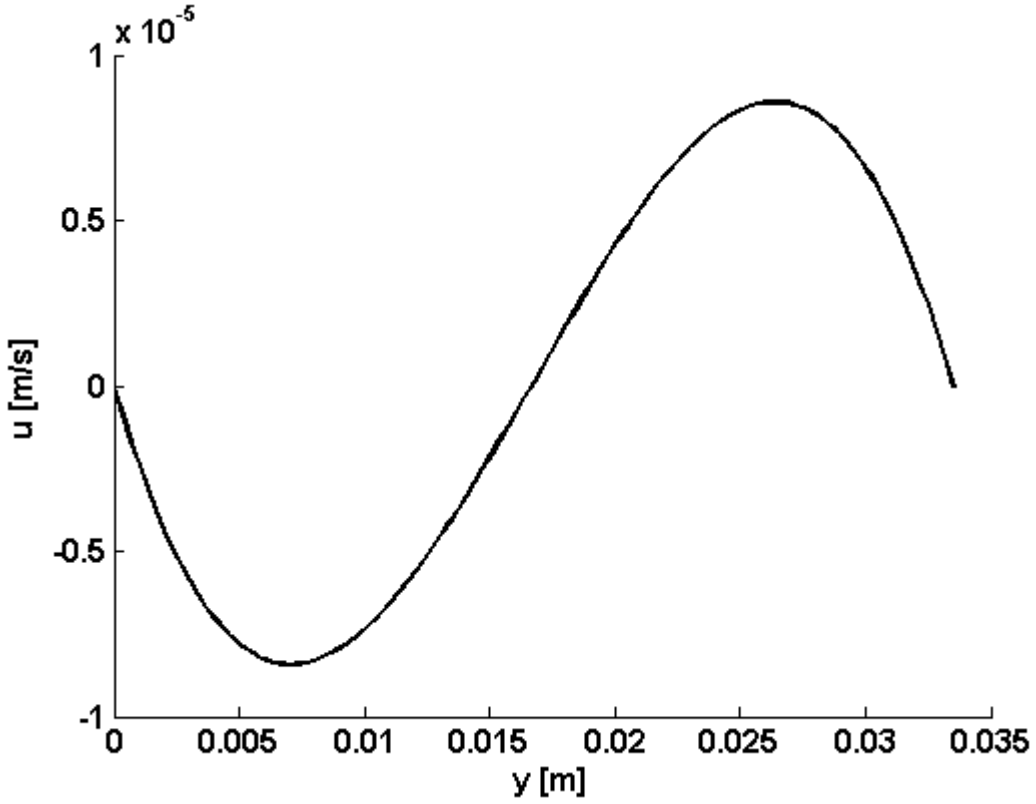

Figure 12.7. Dimensional study for fully filled porous channel, b=33.5 mm, K=0.40 (m^2)

Figure 12.7 shows the same channel of Figure 12.6 but the gap between plates is taken as 33.5 mm. The square bars and gap between square bars are kept the same but the change in gap results in the change of Darcy number. The change of gap between the plates reduces Da number to 9.95×10^{-5}. The velocity decreases due to obstacles in the porous medium. Compared to the Figure 12.6, the velocity along the channel decreases because the distance between the parallel plates is reduced. Darcy number is decreased which means that the fluid cannot flow in the channel easily due to smaller distance between the parallel plates.

Figure 12.8 shows pressure gradient along the channel for different values of Gr_c/Re and the gap between hot and cold plates. The gap is taken as 33.5 and 65 mm. Porosity is taken as 0.40 m^2. As seen from the both lines in Figure 12.8, the pressure gradient along the channel is nearly the same with a change of Gr_p/Re value. However, the pressure gradient increases along the channel with a change of the gap between plates, *b*.

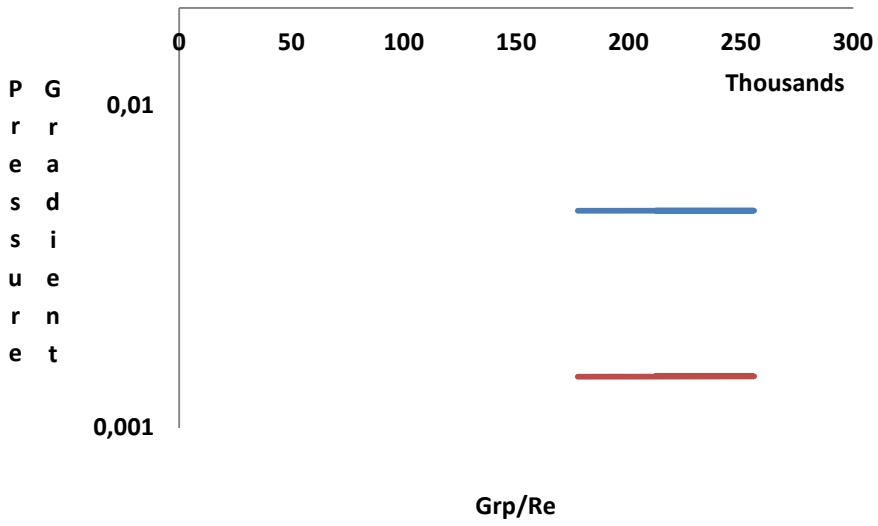

Figure 12.8. Pressure gradient along the fully porous channel

12.2.2. Dimensionless Study

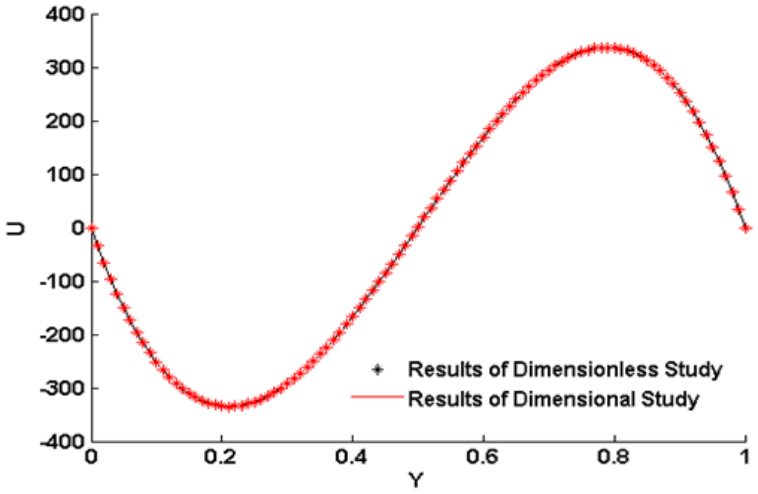

Figure 12.9. Comparison of dimensional and dimensionless study for fully porous channel, $Gr_p/Re=20000$

Figure 12.9 shows comparison of the dimensional and dimensionless study for fully porous channel. Dimensional results given in section 12.2.1 by Figure 12.6 are made using dimensionless parameters given in Equation 7.1. Gr_p/ Re value is calculated as 20000 for aforementioned problem and dimensionless form of Figure 12.6 is presented in Figure 12.9. Analytical expression for velocity distribution (Equation 6.2) and analytical solution of velocity distribution (Equation 7.9) are plotted in Figure 12.9.

As it can be seen on figure, there is a great agreement between dimensional and dimensionless study.

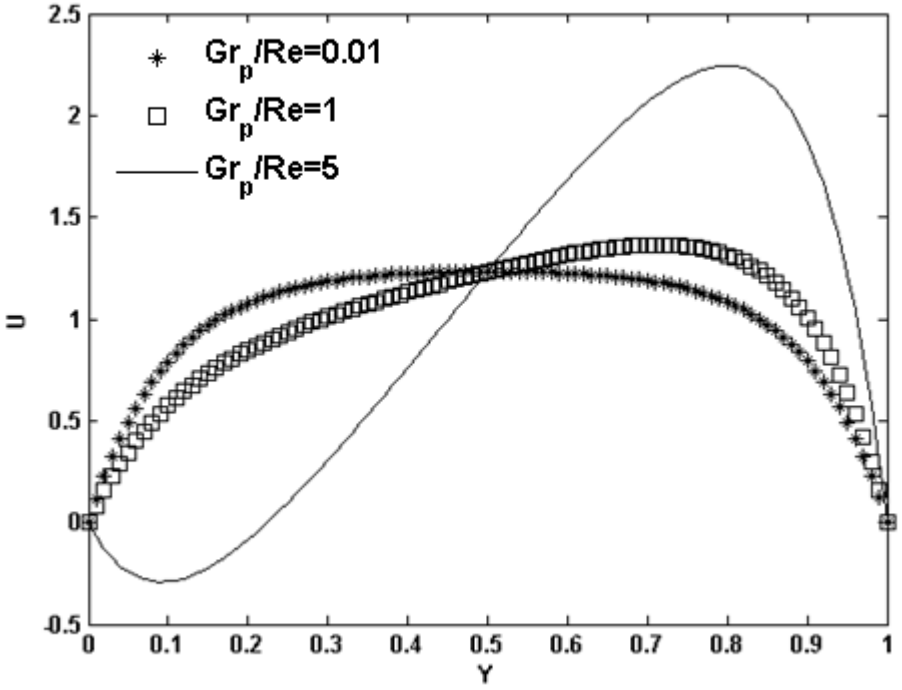

Figure 12.10. The change of velocity profile with Gr_p/Re numbers for fully porous channel while $Da=10^{-2}$, dimensionless study

Figure 12.10 shows the change of dimensionless velocity profiles with different Gr_p/Re values when $Da= 10^{-2}$. As seen on figure, when the force convection is dominant, which means Gr_p/Re value is low, no reversal flow occurs due to negligible buoyancy forces. However, with increasing Gr_p/Re value, which means buoyancy forces becomes effective and natural convection is not negligible anymore, the flow reversals are seen near cold plate while increasing velocity near the hot wall. It should be reminded that a fixed mass flow rate is considered for the all presented results.

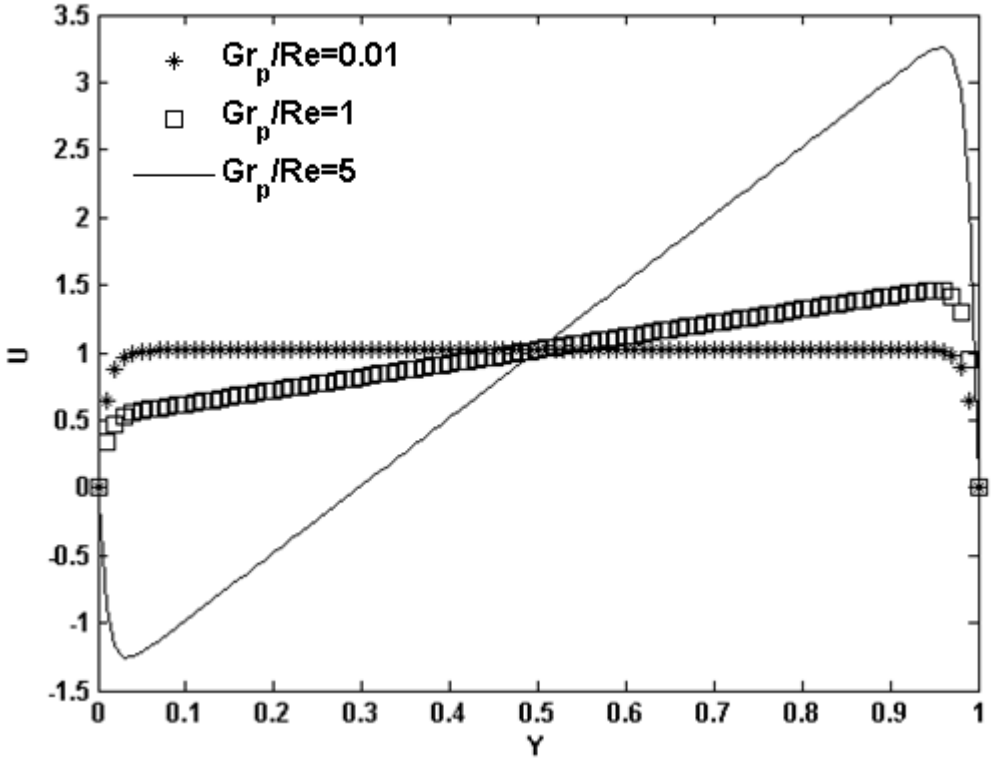

Figure 12.11. The change of velocity profile with Gr_p/Re numbers for fully porous channel while $Da=10^{-4}$, dimensionless study

Figure 12.11 is almost the same with Figure 12.10,but the value of Da is changed as $Da=10^{-4}$. The reduction of Da number from 0.01 to 0.0001 considerably changes the shape of velocity profile, if Figure 12.11 is compared with Figure 12.10. By decrease of Da value, the fluid cannot flow easily in the channel due to denser distribution of obstacles in the channel. Again, as it is seen from Figure 12.10, the dimensionless velocity profile is parabolic for the low values of Gr_p/Re such as value $Gr_p/Re = 0.01$ A parabolic velocity profile is also expected on Figure 12.11,however the velocity profiles become flatten due to obstacles in the channel when $Gr_p/Re=0.01$ and 1.

12.3. Obtained Results for Channel Partially Filled with Porous Medium

In this subsection, results of Chapter 8 and 9 are discussed. The results of dimensionless and dimensional studies are presented. A sample study for different cases of a thermal conductivity ratio is given in Table 12.3. All values are taken for 27 ℃.

Table 12.3. A sample study for thermal conductivity ratio, K

Material	k_{fluid}	k_{solid}	ε	k_{eff}	K
Mercury - Magnesium	8,54	1024	0,4	617,82	0,01
Mercury - Aluminum foil	8,54	0,000017	0,1	0,85	10
Engine Oil - Aluminum foil	0,143	0,000017	0,02	0,003	50
Water - Aluminum foil	0,0263	0,000017	0,01	0,0001	100

12.3.1. Dimensional Study

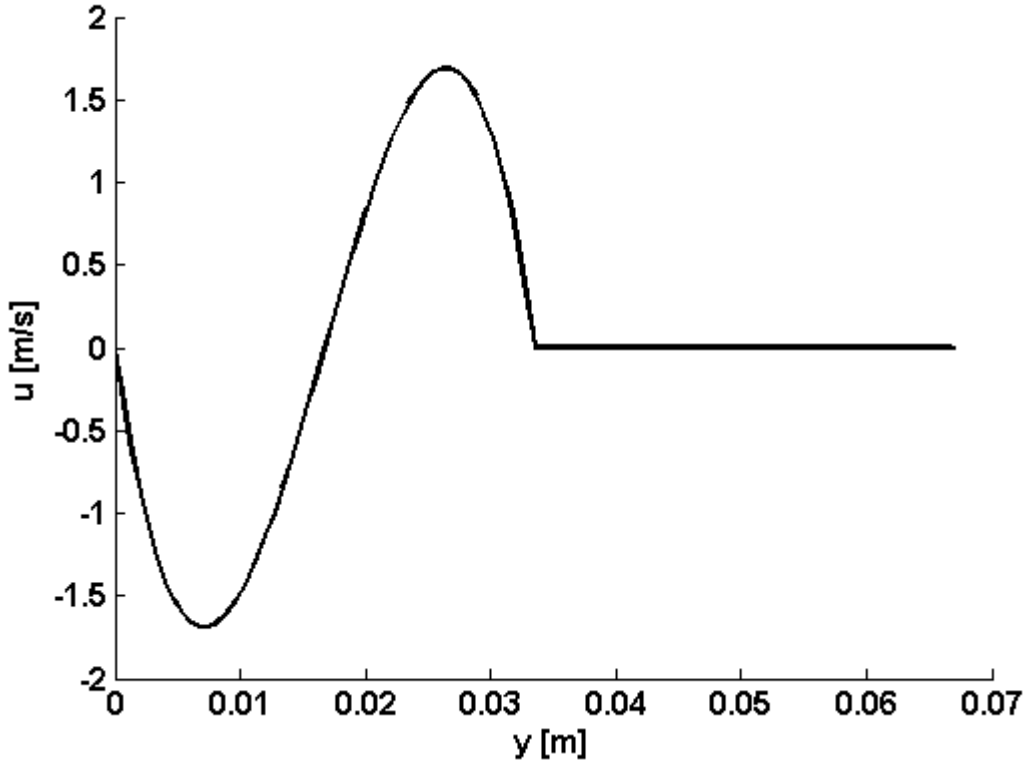

Figure 12.12. Velocity profile of dimensional study for partially filled porous channel while K= $3.7x10^{-4}$, Da = $2.3287x10^{-5}$, Gr_c/Re = $8.45x10^{9}$

Figure 12.12 shows the velocity profile of dimensional study of a partially filled porous channel. The temperatures of the left and right plates are taken as 0^oC and 800^oC respectively. Thermal conductivity ratio (i.e., K) is calculated as $3.7x10^{-4}$, permeability is found as $10.05x10^{-7}$, while the Darcy number is $2.3287x10^{-5}$ and Gr_c/Re ratio is $8.45x10^{9}$. The right half part of the channel is filled with porous medium. The porous material is taken as aluminum. Porosity is calculated as 0.40, thermal conductivity of air is 0.0525 W/mK at film temperature. As it is seen from Figure 12.12, the fluid velocity

in the right half side of the channel is very low due to the obstacles in the channel. However, the fluid can flow easily as there is no restriction or obstacle in the left part of the channel.

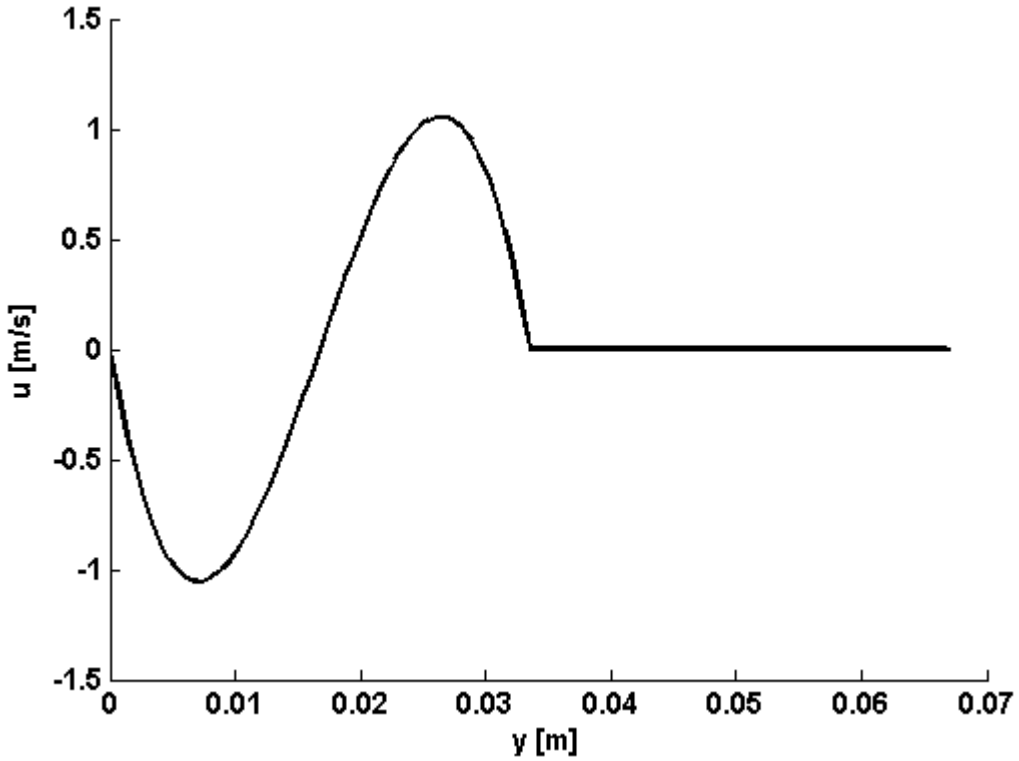

Figure 12.13. Velocity profile of dimensional study for partially filled porous channel while K= 0.6034, Da = 2.3287×10^{-5}, $Gr_c/Re = 8.45 \times 10^{9}$

Figure 12.13 shows the same channel with the Figure 12.12 but this time, the porous material is taken as polystyrene whose thermal conductivity ratio is lower than aluminum. Thermal conductivity ratio (i.e. K) is calculated as 0.6034. Porosity and thermal conductivity ratio of the air is kept constant. Da and Gr_c/Re is also not changed. As it is seen, the change of thermal conductivity ratio affects the velocity profile; velocity is decreased in the channel. The change in thermal conductivity ratio affects the temperature along the channel which affects the buoyancy effect. Therefore, the rate of flow reversal decreases.

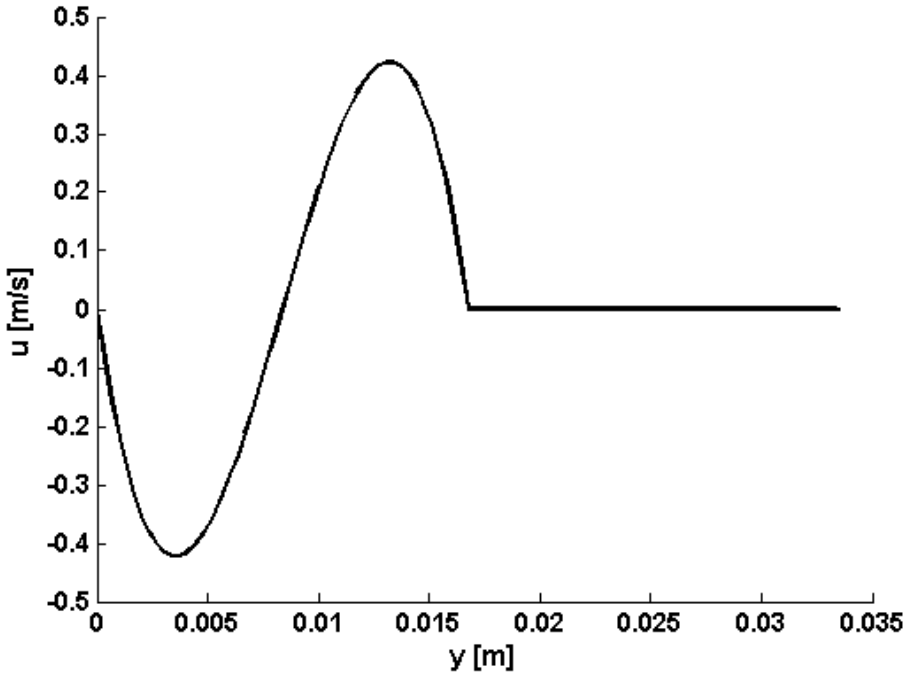

Figure 12.14. Velocity profile of dimensional study for partially filled porous channel while K= 0.6034, Da = 2.3287×10^{-5}, $Gr_c/Re = 2.1213 \times 10^{9}$

The gap between plates is reduced to 33.5 mm in Figure 12.14. All other properties are kept constant with Figure 12.13.Therefore, Figure 12.14 shows that a decrease of the gap between hot and cold plates results in decrease in Gr_c/Re ratio. Thus, this results in decrease of buoyancy effects in the channel. That's why velocity is decreased in the left part of the partially filled channel due to reduced Gr_c/Re compared to Figure 12.13.

12.3.2. Dimensionless Study

Validation of the dimensionless study using numerical methods can be seen on Figure 12.15. Dimensional results given in section 12.3.1 by Figure 12.13 are made using dimensionless parameters given in Equation 7.1. The thermal conductivity ratio K= 0.6034, Da = 2.3287×10^{-5}, $Gr_c/Re = 8.45 \times 10^{9}$ is found and dimensionless form of Figure 12.13 is presented in Figure 12.15. Analytical expression for velocity distribution for clear fluid and porous layer (Equation 4.5 and 6.2) and analytical solution of velocity distribution (Equation 5.2 and 7.9) are plotted in Figure 12.15. A good agreement between dimensional and dimensionless study is observed.

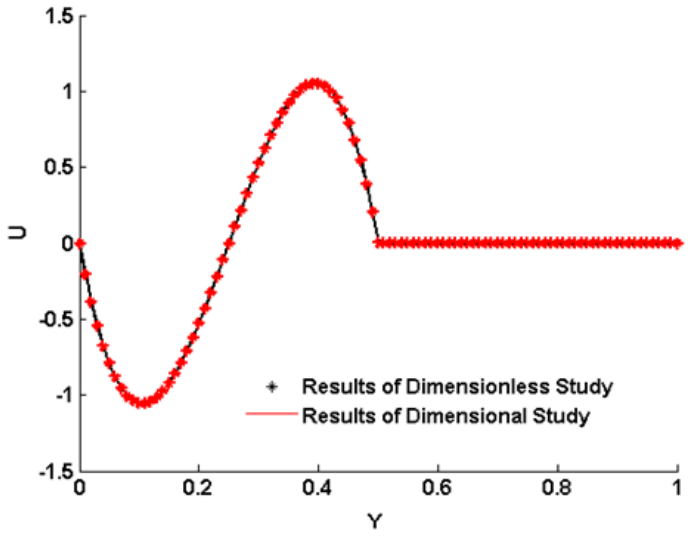

Figure 12.15. Comparison of dimensional and dimensionless study for partially filled porous channel

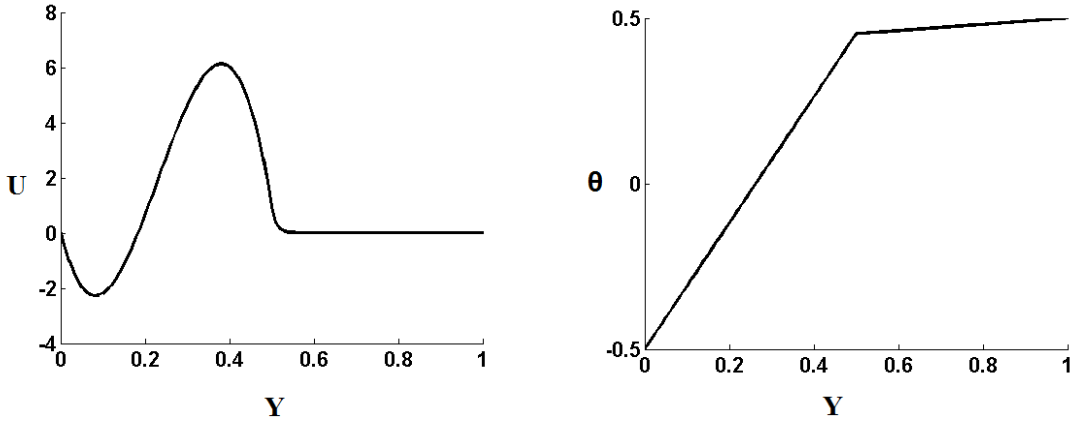

a) b)

Figure 12.16. Velocity profile for partially porous channel, dimensionless study, K=0.05, Da=10^{-4}, Gr_c/Re=2000, a) velocity profile b) temperature distribution

Figure 12.16 shows the dimensionless velocity profile for partially porous filled channel for K=0.05, Da=10^{-4} and Gr_c/Re=2000. The thickness of the porous layer is 0.5 while the channel thickness is 1. As seen from the Figure 12.16, the temperature in the right half of the channel is uniform due to high effective thermal conductivity of porous medium. Consequently, the interface temperature almost same with hot plate and a linear temperature change is observed in the left half of the channel. The velocity is

small in the right region due to low value of Darcy number and a reverse flow occurs in the left half of the channel due to high buoyancy effect.

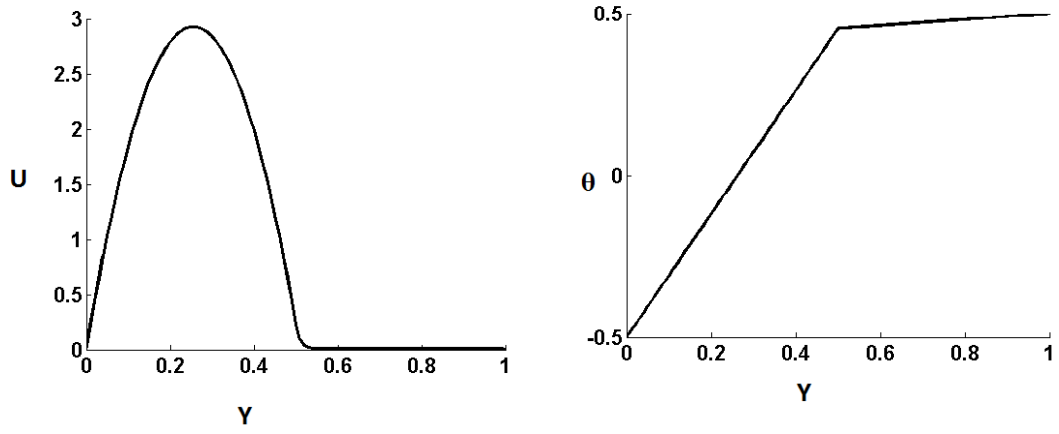

a) b)

Figure 12.17. Velocity profile for partially porous channel, dimensionless study, K=0.05, Da=10-4, Grc/Re=1, a) velocity profile b) temperature distribution

Figure 12.17 shows the velocity profile for channels partially filled with porous medium. The thickness of the porous layer is 0.5 while the channel thickness is 1. The right half of the channel is filled with porous medium while the pure fluid flows in the left half of the channel. Figure 12.17 shows the velocity profile and temperature distribution for the channel with Gr_c/Re= 1, $Da = 10^{-4}$ and $k = 0.05$ which refers to high effective thermal conductivity of porous medium compared to that of clear fluid. As seen from this figure, the right half of the channel, filled with high conductive porous medium, is hot. The value of Gr_c/Re= 1 refers to the strong forced convection heat transfer in the channel. The value of Darcy is low (i.e. 10^{-4}) and that is why a parabolic velocity profile occurs in the left half of the channel. The fluid flow in the right half of the channel is small compared to left side due to the low value of Darcy number.

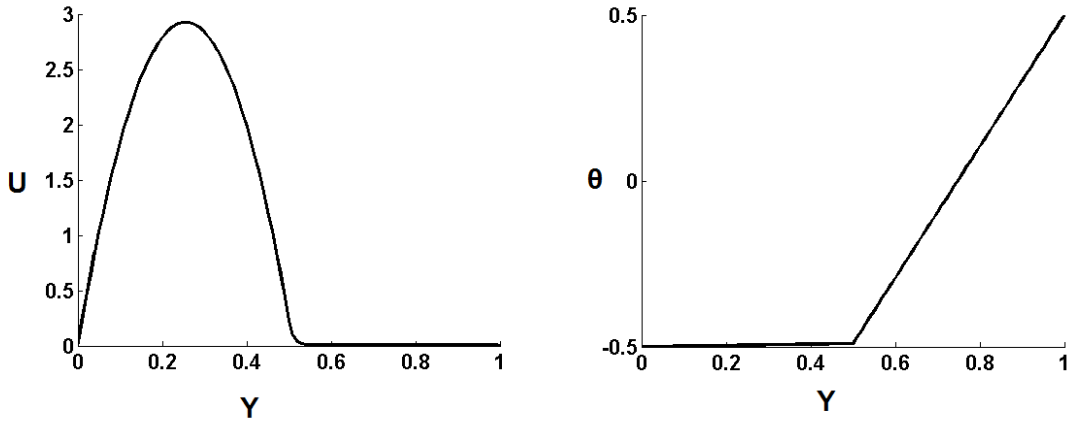

a) b)

Figure 12.18. Velocity profile for partially porous channel, dimensionless study, K=100, Da=10^{-4}, Grc/Re=1, a) velocity profile b) temperature distribution

The velocity profile and temperature distribution in the channel with Gr_c/Re= 1, is shown in Figure 12.18. However, $k = 100$ which refers to high effective thermal conductivity of clear fluid compared to that of porous medium. As seen, a linear temperature distribution is observed in the right half of the channel while temperature is uniform in the left half due to the high thermal conductivity of pure fluid compared to the effective thermal conductivity of porous medium region. The velocity is small in the right half of channel while a parabolic velocity profile is observed in the left half.

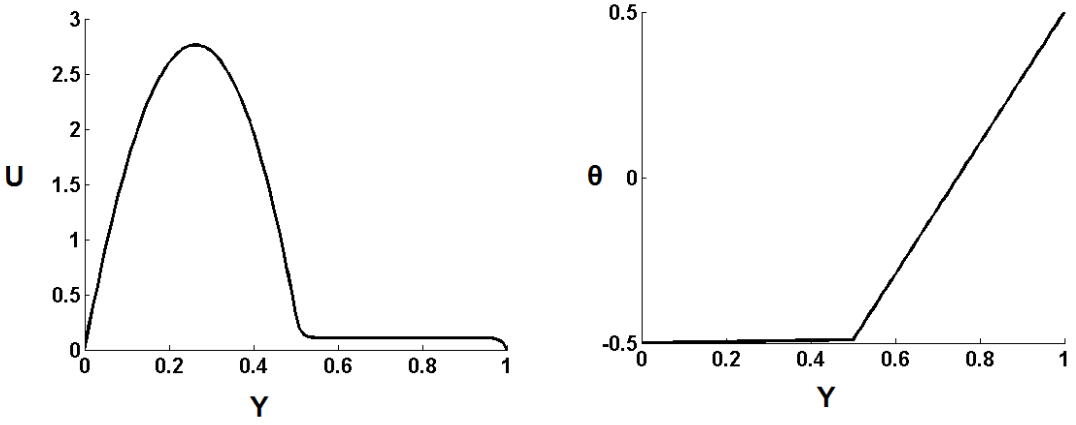

a) b)

Figure 12.19. Velocity profile for partially porous channel, dimensionless study, K=100, Da=10^{-4}, Gr_c/Re=2000, a) velocity profile b) temperature distribution

The parameters of Figure 12.19 are the same with the parameters of Figure 12.18, except Gr_c/Re is 2000 which refers to high buoyancy forces. As seen from Figure 12.19, the temperature linearly changes in the right half of the channel and it is uniform in the left half as θ = -0.5. No buoyancy effect exists in the left half of channel since both the left wall and interface are at θ = -0.5. A parabolic velocity profile occurs in this region due to the fixed inlet mass flow rate.

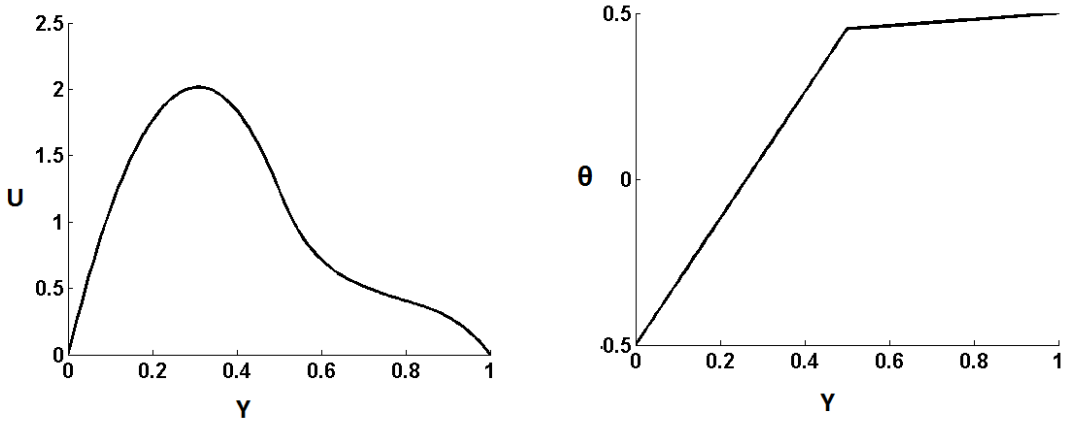

a) b)

Figure 12.20. Velocity profile for partially porous channel, dimensionless study, K=0.05, $Da=10^{-2}$, Gr_c/Re=1, a) velocity profile b) temperature distribution

Figure 12.20 shows the velocity profile for same channels partially filled with porous medium with Figure 12.17. However, in Figure 12.20, Darcy number is increased to 10^{-2}. The thickness of the porous layer is 0.5 while the channel thickness is 1 too and also, the right half of the channel is filled with porous medium while the pure fluid flows in the left half of the channel. Figure 12.20 shows the velocity profile and temperature distribution the channel with Gr_c/Re= 1, and $k = 0.05$ which refers to high effective thermal conductivity of porous medium compared to that of clear fluid. As seen from this figure, the right half of the channel, filled with high conductive porous medium, is hot. The value of Gr_c/Re= 1 refers to the strong forced convection heat transfer in the channel. The value of Darcy is higher than Figure 12.17 that's why flow in the right half of the channel is increased compared to right side of Figure 12.17 due to the increased value of Darcy number.

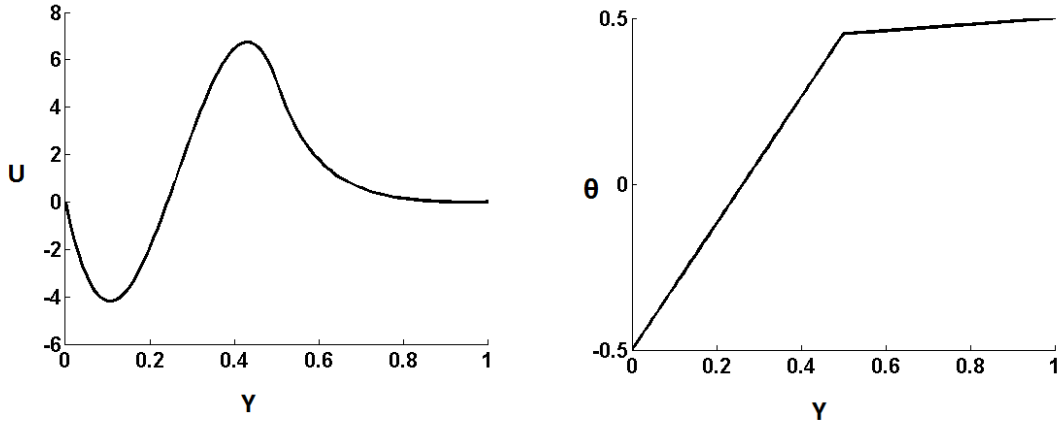

a) b)

Figure 12.21. Velocity profile for partially porous channel, dimensionless study, K=0.05, Da=10^{-2}, Gr_c/Re=2000, a) velocity profile b) temperature distribution

Figure 12.21 shows the dimensionless velocity profile for partially porous filled channel for K=0.05, Da=10^{-2} and Gr_c/Re=2000. The channel and assumptions are same. However, in Figure 12.21, Darcy number is increased to 10^{-2} from 10^{-4}. As seen from the Figure 12.21, the temperature in the right half of the channel is uniform due to high effective thermal conductivity of porous medium. Consequently, the interface temperature almost same with hot plate and a linear temperature change is observed in the left half of the channel. The velocity is increased in the right region due to higher value of Darcy number and that's why a reverse flow occurs in the left half of the channel is higher due to high buoyancy effect and higher Darcy number.

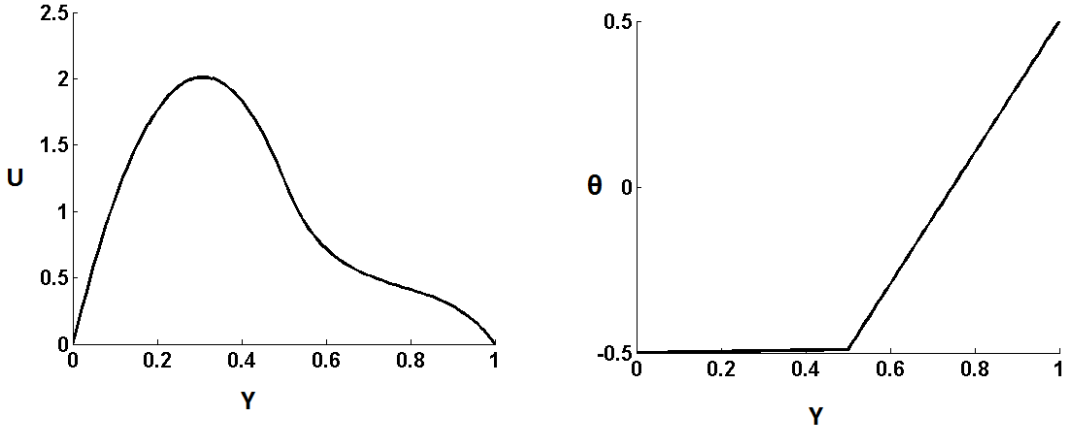

a) b)

Figure 12.22. Velocity profile for partially porous channel, dimensionless study, K=100, Da=10^{-2}, Gr_c/Re=1, a) velocity profile b) temperature distribution

Figure 12.22 is same study with Figure 12.18 with a difference of Darcy number. As it is seen, an increase in Darcy number results in fluid flows easier on the right half of the channel. That's why velocity increases in the right half of the channel.

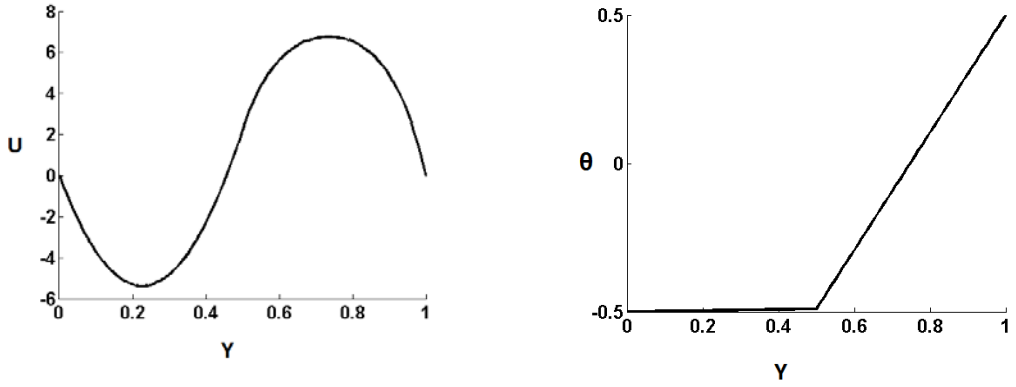

a) b)

Figure 12.23. Velocity profile for partially porous channel, dimensionless study, K=100, Da=10^{-2}, Gr_c/Re=2000, a) velocity profile b) temperature distribution

The parameters of Figure 12.23 are the same with the parameters of Figure 12.19, except Darcy number which is 10^{-2}. As seen from Figure 12.23, the temperature linearly changes in the right half of the channel and it is uniform in the left half as θ = -0.5. Buoyancy effect exists in the left half of channel since Darcy number is increased

compared to the Figure 12.19. This results in increase of velocity in the right half of the channel.

12.4. Heatline Patterns

12.4.1. Results and Discussion

Both numerical and analytical results (the velocity profile, temperature and heatfunction distribution) were found and compared for all presented results. The numerical and analytical results are identical when 101x101 number of nodes is used in the numerical approach. Furthermore, the velocity profiles are also compared with the profiles reported in literature. For instance, the velocity profiles of the present work and the profiles reported by Aung and Worku (1986) for the channels with clear fluid and by Degan and Vasseur (2002) for the channels filled with fluid saturated porous medium are compared and good agreement between the results are observed.

12.4.2. Heatline Patterns in the Channel with Pure Fluid Flow

Figure 12.24 shows the velocity profile, temperature distribution and heatline patterns in a channel with two values of Gr_c / Re of 1 and 400, and three Peclet numbers of 0.01, 1 and 5. The velocity profile and temperature distribution are shown in the first columns while the heatline patterns are in the second, the third and fourth columns for three Peclet numbers of 0.01, 1 and 5, respectively. The velocity profile, temperature distribution and heatline patterns for the channel with Gr_c / Re =1 are shown in the first column of Figure 12.24(a). Forced convection is dominant and velocity profile is almost parabolic and a linear temperature variation exits in the channel. The heatline patterns in the channel with Peclet number of 0.01 are not affected from fluid flow and heat path is almost horizontal. By increasing of Peclet number from 0.01 to 1, the heatline patterns are considerably changed and the convection heat transfer becomes stronger. For Pe = 1, the heatlines are not horizontal and the effect of vertical convection transport can be observed. The convection heat transport in vertical direction is improved for the channel with Pe = 5. Heat takes a long distance in vertical direction to be transferred from the right to left wall. It should be mentioned that the maximum heatfunction value at the left

wall, showing the dimensionless heat transfer from the right to left wall, is $H_{max} = 2$ for three Peclet numbers, as expected. Figure 12.24(b) shows the velocity profile, temperature distribution, and heatline patterns in a channel with $Gr_c / Re = 400$ for the same Peclet numbers of Figure 12.24(a). The increase of Gr_c / Re ratio, increases mass flow in upward direction and that is why a reverse flow occurs in the channel. The comparison of Figure 12.24(a) and 12.24(b) shows that the change of velocity profile in the channel does not affect heatline distribution in the channel for Pe = 0.01 since the conduction heat transfer from the right to left wall is the dominant mode of heat transport between two plates and heat moves horizontally from the right to left wall. For Pe = 1, the effects of the convection mode of heat transport and the effect of reverse flows on heatline patterns can be observed. Heat is separated from the right wall and goes in upward direction due to the strong convection. After a distance, the direction of heat transport is changed and heat flows in downward direction due to the reverse flow and finally it is received by the left wall. Further distortion of heatline patterns can be observed in the channel with Pe = 5. In the channels with high value of Peclet number (i.e., Pe = 5), for which convective heat transport is dominant, heatline patterns are highly affected from fluid flow. It should be mentioned that for the clear fluid channel with $Gr_c / Re = 400$, the dimensionless heat transfer rate is 2 since a linear temperature distribution exists in the channel.

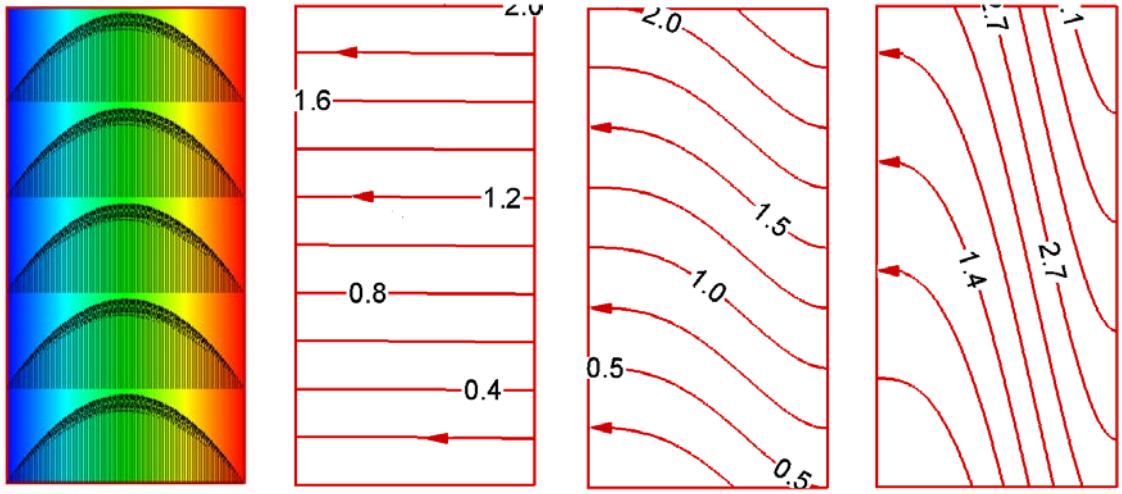

Pe=0.01 Pe=1 Pe=5

(a)

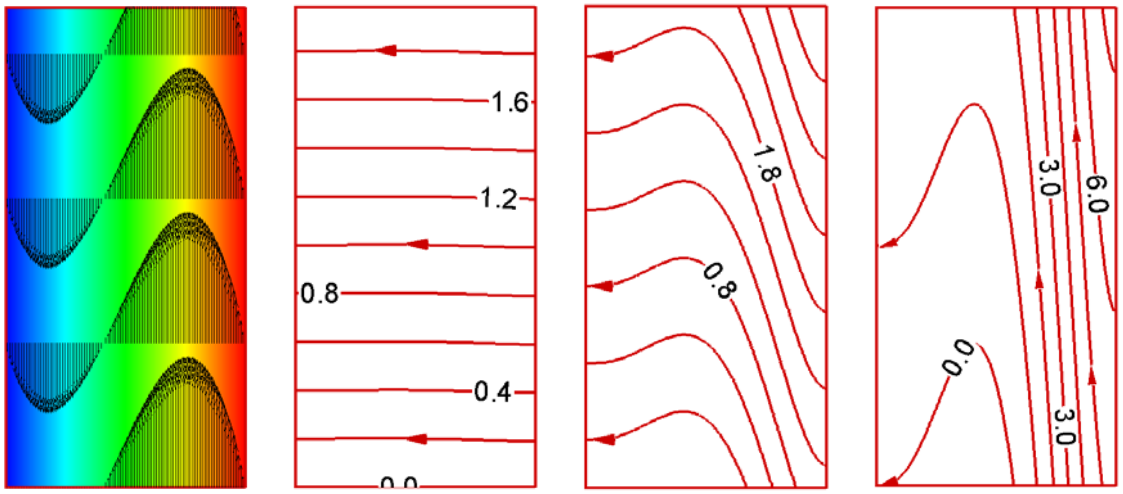

Pe =0.01 Pe=1 Pe=5

(b)

Figure 12.24. Velocity profile (the first column) , temperature profile (the second column) and heatline patterns for Pe = 0.01, 1 and 5 (the third, fourth and fifth columns, respectively) in channel with clear fluid, a) Gr_c/Re = 1, b) Gr_c/Re =400

12.4.3. Heatline Patterns in the Channel Filled with Fluid Saturated Porous Media

Figure 12.25 shows the velocity profile, temperature distribution and heatline patterns in a porous medium filled channel with $Da = 10^{-4}$ and two values of Gr_p / Re

as 0.01 and 5. It shows the heatline patterns for three Peclet numbers of 0.01, 1 and 5. Similar to the Figure 12.24(a), for low values of Gr_p / Re = 0.01, forced convection is dominant and a symmetrical velocity profile is observed in the channel. For the low values of Peclet number (i.e. Pe = 0.01), the conduction mode of heat transfer from the right to left wall is dominant and heat flows horizontally. By increasing of Peclet number from 0.01 to 1.0, the convection in vertical direction affects heatline patterns and heat separated from the right wall takes a vertical distance to be received by the left wall. The effect of vertical flow on heatline patterns is clearly observed in the channel with Pe = 5 in which a strong convective transport exists. Figure 12.25(b) shows that by increasing of Gr_p / Re from 0.01 to 5, a reverse flow occurs in the channel. This reversal flow does not affect heatline patterns for the channel with Pe = 0.01 due to strong heat conduction from the right to left wall. However, the heatline distribution in the channel with Pe = 5 is highly influenced from the reverse flow due to the encountering effect of convection heat transport in vertical direction.

Figure 12.26 compares the velocity and heatline patterns in the channel with clear fluid ($Gr_c / Re = 1$) and the channel completely filled with saturated fluid porous medium ($Gr_p / \mathrm{Re} = 0.01, Da = 10^{-4}$) when Pe = 5. The velocity profile of the channel with completely porous medium is flattened due to the obstacles in the porous medium. The temperature variation for both channels is identical, and temperature linearly changes from right to the left wall. Figure 12.26(b) compares the heatline patterns of the both channels. As seen, there is difference in heatline patterns due to small changes in the velocity profiles. This figure shows that for high values of Peclet number, how the small changes in velocity profile can affect heatline patterns.

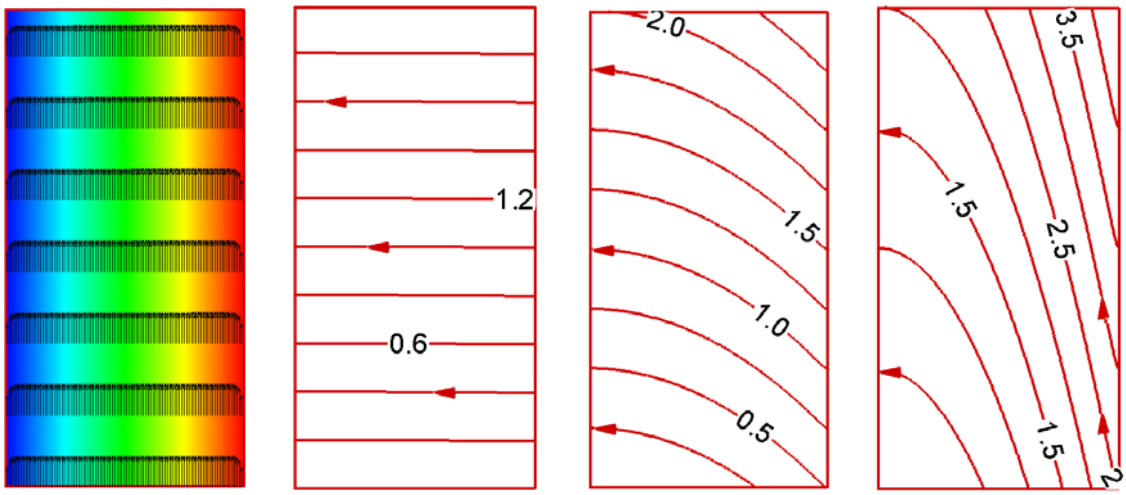

Pe =0.01 Pe=1 Pe=5

(a)

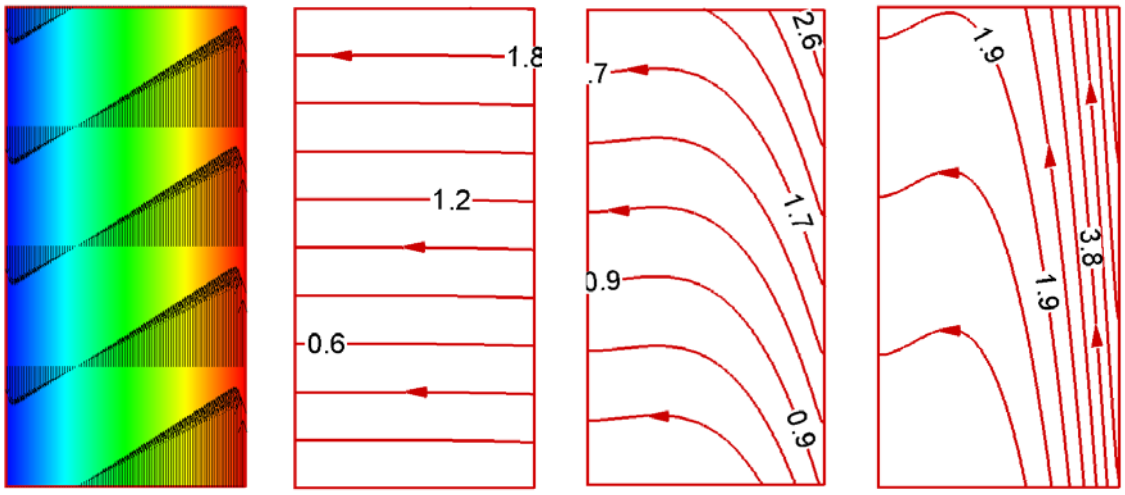

Pe =0.01 Pe=1 Pe=5

(b)

Figure 12.25. Velocity profile (the first column) , temperature profile (the second column) and heatline patterns for Pe = 0.01, 1 and 5 (the third, fourth and fifth columns, respectively) in channel filled with saturated porous medium, a) $Gr_p/Re = 0.01$, b) $Gr_p/Re = 5$

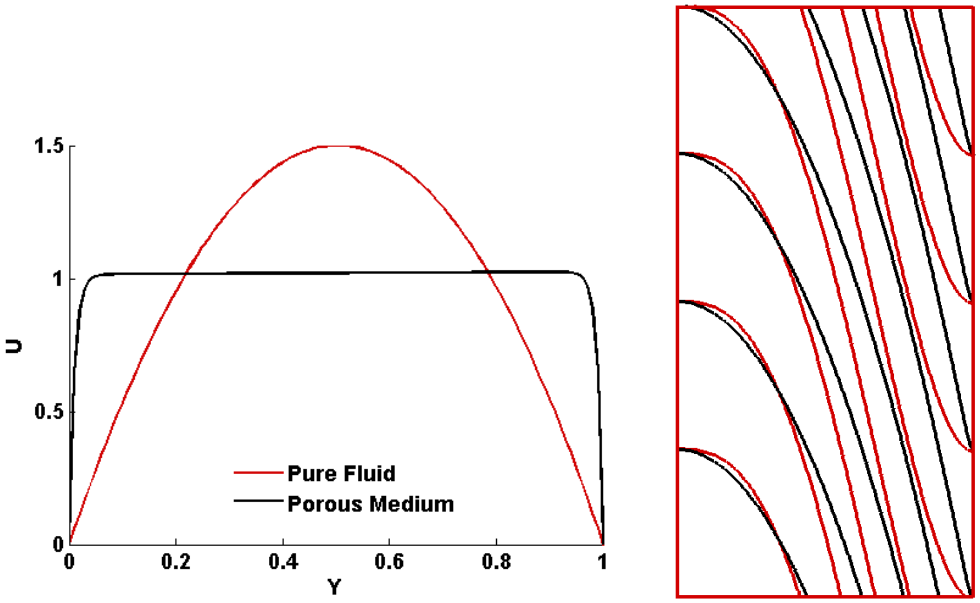

(a) (b)

Figure 12.26. Comparison of heatline for clear fluid ($Gr_c/Re=1$) and completely porous medium channel ($Gr_p/Re = 0.01$, $Da=10^{-4}$) when Pe = 5 a) velocity profile b) heatline patterns

12.4.4. Heatlines Patterns in the Channel Partially Filled with Saturated Porous Media

Figure 12.27 shows the velocity profile, temperature distribution and heatline patterns for channels partially filled with porous medium. The thickness of the porous layer is 0.5 while the channel thickness is 1. The right half of the channel is filled with porous medium while the pure fluid flows in the left half of the channel. Figure 12.27(a) shows the velocity profile, temperature distribution an heatline patterns for the channel with $Gr_c / \mathrm{Re} = 1$, $Da = 10^{-4}$ and $k = 0.05$ which refers to high effective thermal conductivity of porous medium compared to that of clear fluid. As seen from this figure, the right half of the channel, filled with high conductive porous medium, is hot (θ = 0.5) and temperature is almost uniform. The dimensionless temperature is linearly changes from 0.5 to -0.5 in the right half of the channel. The value of $Gr_c / \mathrm{Re} = 1$ refers to the strong forced convection heat transfer in the channel. The value of Darcy is low (i.e. $Da = 10^{-4}$) and that is why a parabolic velocity profile occurs in the left half of the channel. The fluid flow in the right half of the channel is small compared to left side due to the low value of Darcy number. For Pe = 0.01, the conduction mode of heat transfer from the right to left wall is dominant and that is why heat flows horizontally from the hot to cold wall. By increasing of Peclet number from 0.01 to 1, the direction of heat flow in the right half region is not changed. The convection strength in vertical direction is weak while the conduction heat transport from the right wall to the interface is strong. That is why, heat flows horizontally in the right half of channel. In the left half of the channel, the effect of convection heat transfer in vertical direction is considerably higher that the conduction heat transfer in horizontal direction. The path of heat transfer is changed in the left region of channel. Heat flows upward due to the strong convection effect while it flows towards the cold wall and finally it is received by the left wall. By increasing of Peclet number from 1 to 5, the heat path does not change in the right half of the channel due to the strong conduction mode of heat transfer from the right wall toward the interface. However, in the left half of region, heat takes a longer distance in vertical direction due to the strong convection heat transfer in vertical direction. The maximum value of dimensionless heatfunction at the left wall is 3.81 indicating that by inserting of high conductive porous layer heat transfer rate from the right to left increase.

The velocity profile, temperature distribution and heat flow patterns in the channel with Gr_c / Re = 1, $Da = 10^{-4}$ and $K = 100$ are shown in Figure 12.27(b). The heatline patterns are plotted for three different Peclet numbers of 0.01, 1 and 5. As seen from the first column, a linear temperature distribution is observed in the right half of the channel while temperature is uniform in the left half (i.e., θ = -0.5) due to the high thermal conductivity of pure fluid compared to the effective thermal conductivity of porous medium region. The velocity is small in the right half of channel while a parabolic velocity profile is observed in the left half. For low Peclet number of 0.01, the heat flow is horizontal from the hot to cold wall. For Pe = 1, in the right half of channel, the conduction heat transport in horizontal direction from the right wall to interface is weak and it is comparable with convective heat transport in the vertical direction. That is why; heat separated from the right wall moves vertically due to the convective heat transport and then it moves toward the interface. In the left half of channel, the convection heat transport in vertical direction (i.e., thermal energy transported in vertical direction) is comparable with the conduction heat transport in horizontal direction since the fluid thermal conductivity is high. Hence, heat moves vertically when it moves toward the left wall. By increasing Peclet number from 1 to 5, the same heat transport paths are valid. However, the heatlines becomes more vertically due to the stronger convection heat transport in vertical direction. The maximum dimensionless heatfunction at the left wall is 0.04 showing inserting of porous layer with low thermal conductivity reduces heat transfer between walls.

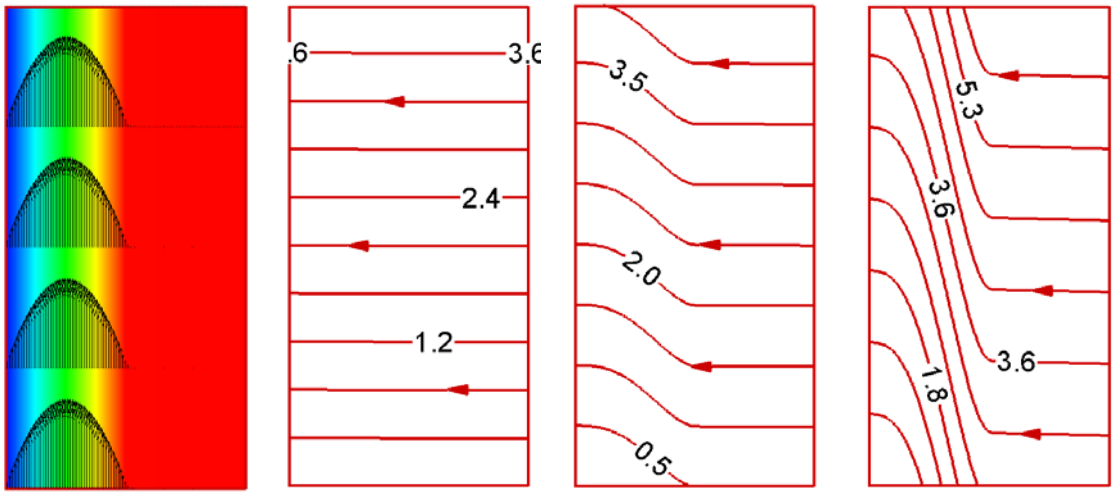

Pe=0.01 Pe=1 Pe=5

(a)

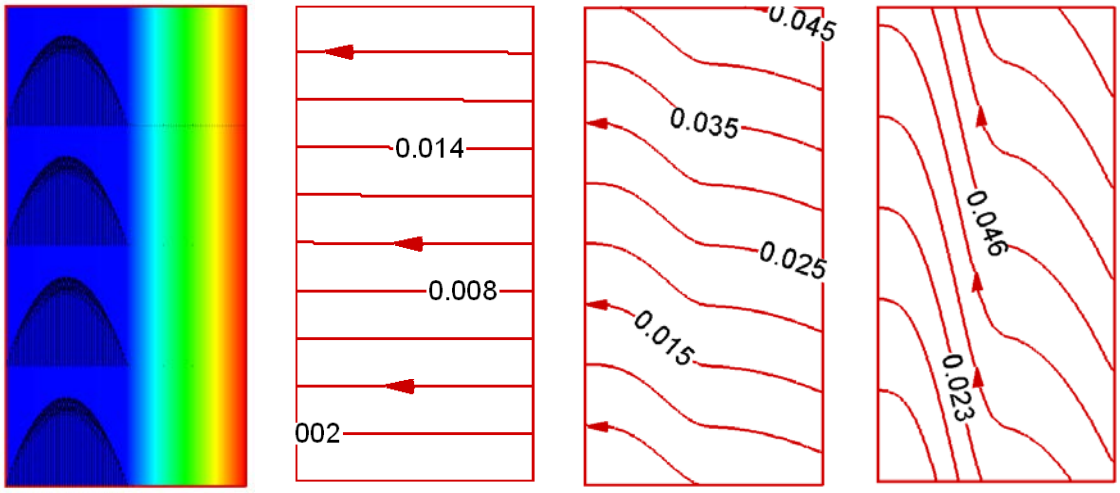

Pe=0.01 Pe=1 Pe=5

(b)

Figure 12.27. Velocity profile (the first column) , temperature profile (the second column) and heatline patterns for Pe = 0.01, 1 and 5 (the third, fourth and fifth columns, respectively) in channel filled with saturated porous medium, Gr_c/Re= 1, Da=10^{-4} a) K = 0.05, b) K=100

Figure 12.28(a) shows the velocity profile, temperature distribution and heatline patterns in the channel with $Gr_c / \mathrm{Re} = 2000$ and $Da = 10^{-4}$ when $k = 0.05$. Similar to the Figure 12.26, the heatline patterns are plotted for Peclet numbers of 0.01,1 and 5. As seen from the first column of the Figure 12.28(a), the temperature in the right half of the channel is uniform as θ = 0.5 due to high effective thermal conductivity of porous

medium. Consequently, the interface temperature is $\theta = 0.5$ and a linear temperature change is observed in the left half of the channel. The velocity is small in the right region due to low value of Darcy number and a reverse flow occurs in the left half of the channel due to high buoyancy effect. The second column of Figure 12.28(a) shows heatline patterns in the channel when Pe = 0.01. As expected, heat is transported horizontally from the hot to the cold wall for Pe = 0.01. For Pe = 1, heat transfers horizontally in the right half of the channel is comparable with due to the considerable conduction heat transport from the right wall to the interface. Then, it moves upward in the left half of the channel due to the strong convective heat transport and attains a maximum point. After this point, heat moves downward due to the reverse flow occurs in the region close to the cold wall. By increasing of Peclet number from 1 to 5, the effect of convection heat transfer in vertical direction increases and heat moves a long distance in the vertical direction in the left half of the channel.

The parameters of Figure 12.28(b) are the same with the parameters of Figure 12.27(b), except thermal conductivity ratio which is 0.01 refers to low thermal conductivity of the right half compared to the left one. As seen from the first column of Figure 12.28(b), the temperature linearly changes in the right half of the channel and it is uniform in the left half as $\theta = -0.5$. No buoyancy effect exists in the left half of channel since both the left wall and interface are at $\theta = -0.5$. A parabolic velocity profile occurs in this region due to the fixed inlet mass flow rate. For Pe = 0.01, as expected, the heat transport is horizontally. For Pe = 1, in the right region, the convection heat transport in vertical direction is higher than conduction heat transport in horizontal direction. It should be reminded that in the right half of the channel, the conduction heat transfer from the right wall to the interface is weak due to the low effective thermal conductivity of porous medium. That is why; heat moves a distance in vertical direction when it goes towards the interface. After passing of heat from the interface, in the left half of the channel, heat moves more horizontally due to high conduction heat transfer from the interface to the left wall. The same comments are valid for the channel with Pe = 5, however the effect of upward flow on heatline patterns increases as seen from the fourth column of Figure 12.28(b).

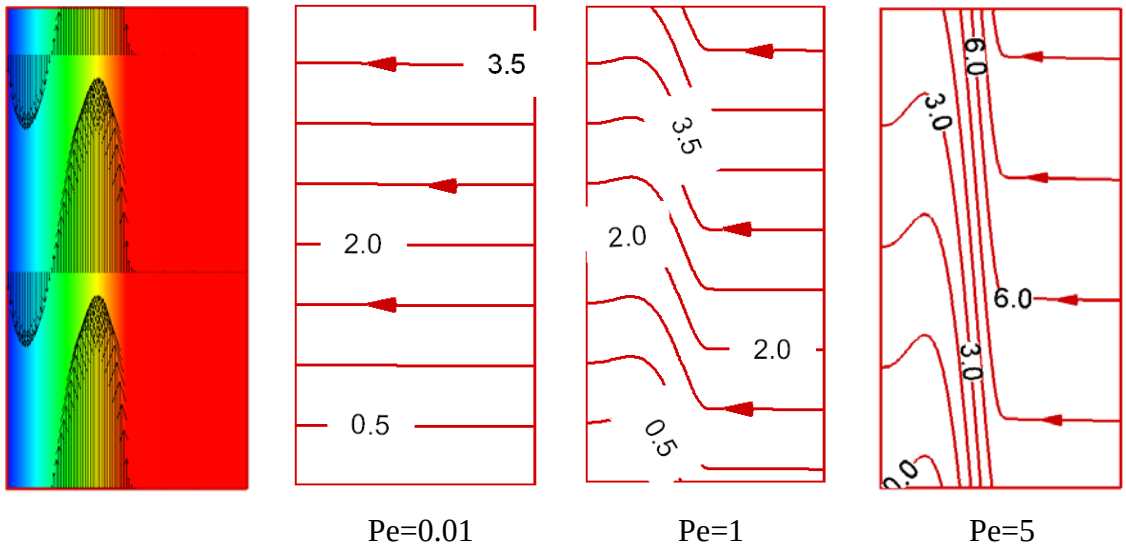

Pe=0.01 Pe=1 Pe=5

(a)

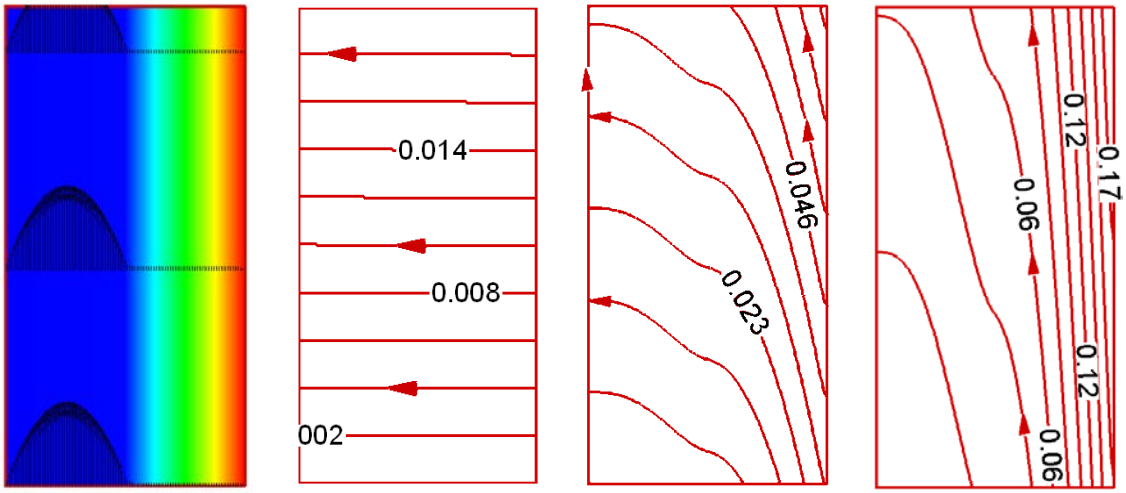

Pe=0.01 Pe=1 Pe = 5

(b)

Figure 12.28. Velocity profile (the first column) , temperature profile (the second column) and heatline patterns for Pe = 0.01, 1 and 5 (the third, fourth and fifth columns, respectively) in channel filled with saturated porous medium, $Gr_c/Re=2000$, $Da=10^{-4}$ a) K = 0.05, b) K=100

CHAPTER 13

CONCLUSION

In this thesis, heat transfer enhancement in a vertical channel filled with a clear fluid, fully porous media and partially porous media is investigated. Firstly, fluid and heat flow in clear channel is solved both dimensional for a specific case and dimensionless and analytical expressions are given in separate sections. Following analytical expressions, each problem is solved dimensional and dimensionless numerically. Dimensional results are compared with analytical equations and dimensionless numerical results. As it is given in Chapter 12, a great agreement between analytical and numerical results is obtained between each solution. All these steps are done for each studied case; clear fluid channel (Chapter 4 and 5), fully porous channel (Chapter 6 and 7) and partially filled channel (Chapter 8 and 9) as they are explained in separate chapters.

The occurrence of flow reversals along the channel is highly affected by a change of Gr/Re value. Increase of Gr/Re value increases the possibility of flow reversals, as buoyancy force gets effective along the channel and therefore, flow reversal occurs due to fixed flow rate. Another conclusion can be made is porous media decreases the possibility of flow reversal occurrence. For instance, in pure fluid channel, 0 ^{o}C and 100 ^{o}C cold and hot plate temperatures respectively is enough to visualize flow reversals in the channel. However, the hot plate temperature should be increased to 800 ^{o}C in completely and partially filled porous channels to visualize flow reversals in the channel. It also can be concluded that it is possible to prevent flow reversals by using porous media in the channel.

Following to obtaining velocity profiles by solving momentum equations, two dimensional heatfunctions are solved to obtain heat transport along the channel. It is observed that the use of heatfunction concept can explain the competition between the horizontal conduction heat transport and vertical convection mode of heat transfer in the channel. The equations needed to be solved to visualize heat transport are explained in a detail in Chapter 10.

Several conclusions can be made about heat transport along the channel. First of all, Peclet number is one of the parameters that affect heat transfer along the channel. For low Peclet numbers, heatline patterns are horizontal while heatline patterns take a vertical distance along the channel. The heat transfer is highly affected by velocity profile at high Peclet numbers since convection is the main driven mechanism. However, at low Peclet numbers, velocity profile does not affect heat patterns since conduction is the main driven heat transfer mechanism. What is more, the use of heatfunction for analyzing of heat and fluid flow problems also shows the dimensionless heat transfer rate through the channel. Thus, the increase or decrease of heat transfer through the channel can be predicted.

REFERENCES

Al-Hadhrami, A. K., Elliott, L., & Ingham, D. B. (2002). Combined Free and Forced Convection in Vertical Channels of Porous Media. *Transport in Porous Media, 49*(3), 265-289.

Aung, W., & Worku, G. (1986). Theory of Fully Developed, Combined Convection Including Flow Reversal. *Journal of Heat Transfer, 108*(2), 485-488.

Aung, W., & Worku, G. (1987). Mixed Convection in Ducts with Asymmetric Wall Heat Fluxes. *Journal of Heat Transfer-Transactions of the Asme, 109*(4), 947-951.

Barletta, A., Magyari, E., Pop, I., & Storesletten, L. (2007). Mixed convection with viscous dissipation in a vertical channel filled with a porous medium. *Acta Mechanica, 194*(1), 123-140.

Barletta, A., & Nield, D. (2009). Combined Forced and Free Convective Flow in a Vertical Porous Channel: The Effects of Viscous Dissipation and Pressure Work. *Transport in Porous Media, 79*(3), 319-334.

Basak, T., Roy, S., Ramakrishna, D., & Pop, I. (2010). Visualization of Heat Transport during Natural Convection within Porous Triangular Cavities Via Heatline Approach. *Numerical Heat Transfer Part a-Applications, 57*(6), 431-452.

Chang, W.-J., & Chang, W.-L. (1995). Mixed convection in a vertical tube partially filled with porous medium. *Numerical Heat Transfer, Part A: Applications, 28*(6), 739-754.

Costa, V. A. F. (1999). Unification of the streamline, heatline and massline methods for the visualization of two-dimensional transport phenomena. *International Journal of Heat and Mass Transfer, 42*(1), 27-33.

Hakyemez, E., Mobedi, M., & Oztop, H. F. (2008). Effects of wall-located heat barrier on conjugate conduction/natural-convection heat transfer and fluid flow in enclosures. *Numerical Heat Transfer Part a-Applications, 54*(2), 197-220.

Incropera, F. P., & DeWitt, D. P. (2007). *Fundamentals of heat and mass transfer*: John Wiley.

Kakaç, S., & Yener, Y. (1995). *Convective Heat Transfer*: CRC Press.

Kaluri, R. S., Anandalakshmi, R., & Basak, T. (2010). Bejan's heatline analysis of natural convection in right-angled triangular enclosures: Effects of aspect-ratio and thermal boundary conditions. *International Journal of Thermal Sciences, 49*(9), 1576-1592.

Kaluri, R. S., & Basak, T. (2010). Heatline analysis of thermal mixing due to natural convection in discretely heated porous cavities filled with various fluids. *Chemical Engineering Science, 65*(6), 2132-2152.

Kaluri, R. S., Basak, T., & Roy, S. (2009). Bejan's Heatlines and Numerical Visualization of Heat Flow and Thermal Mixing in Various Differentially Heated Porous Square Cavities. *Numerical Heat Transfer Part a-Applications, 55*(5), 487-516.

Kimura, S., & Bejan, A. (1983). The Heatline Visualization of Convective Heat-Transfer. *Journal of Heat Transfer-Transactions of the Asme, 105*(4), 916-919.

Kumar, J., Umavathi, J., Pop, I., & Biradar, B. (2009). Fully Developed Mixed Convection Flow in a Vertical Channel Containing Porous and Fluid Layer with Isothermal or Isoflux Boundaries. *Transport in Porous Media, 80*(1), 117-135.

Lai, F. C., Prasad, V., & Kulacki, F. A. (1988). Aiding and opposing mixed convection in a vertical porous layer with a finite wall heat source. *International Journal of Heat and Mass Transfer, 31*(5), 1049-1061.

Mobedi, M. (2008). Conjugate natural convection in a square cavity with finite thickness horizontal walls. *International Communications in Heat and Mass Transfer, 35*(4), 503-513.

Mobedi, M., Ozkol, U., & Sunden, B. (2010). Visualization of diffusion and convection heat transport in a square cavity with natural convection. *International Journal of Heat and Mass Transfer, 53*(1-3), 99-109.

Morega, A. M., & Bejan, A. (1993). Heatline Visualization of Forced-Convection Laminar Boundary-Layers. *International Journal of Heat and Mass Transfer, 36*(16), 3957-3966.

Nield, D. A., & Bejan, A. (2006). *Convection in Porous Media*: Springer.

Parang, M., & Keyhani, M. (1987). Boundary effects in laminar mixed convection flow through an annular porous medium. *Journal of Heat Transfer 109:4*, 1039-1041.

Sparrow, E. M., Chrysler, G. M., & Azevedo, L. F. (1984). Observed Flow Reversals and Measured-Predicted Nusselt Numbers for Natural Convection in a One-Sided Heated Vertical Channel. *Journal of Heat Transfer, 106*(2), 325-332.

Umavathi, J., Kumar, J., Chamkha, A., & Pop, I. (2005). Mixed Convection in a Vertical Porous Channel. *Transport in Porous Media, 61*(3), 315-335.

Varol, Y., Oztop, H. F., Mobedi, M., & Pop, I. (2010). Visualization of heat flow using Bejan's heatline due to natural convection of water near 4 degrees C in thick walled porous cavity. *International Journal of Heat and Mass Transfer, 53*(9-10), 1691-1698.

Waheed, M. A. (2009). Heatfunction Formulation of Thermal Convection in Rectangular Enclosures Filled with Porous Media. *Numerical Heat Transfer Part a-Applications, 55*(2), 185-204.

APPENDIX A

CONSTANTS

$$C_1 = \frac{Gr_p}{\mathrm{Re}},\ C_2 = -csc\,h(S)(\frac{Gr_p}{2Re} + Da\Gamma),\ C_3 = -\csc h(S)(\frac{Gr_p}{2\,\mathrm{Re}} - Da\Gamma),$$

$$C_4 = -\frac{Gr_p}{2\,Re} - Da\Gamma\ ,$$

$$C_5 = \frac{Gr_c\theta_i}{12\,\mathrm{Re}} - \frac{Gr_c}{12\,\mathrm{Re}},\qquad C_6 = \frac{Gr_c}{6\,Re} - \frac{Gr_c\theta_i}{6\,Re} + \frac{Gr_c(2\theta_i+1)}{12\,Re},\qquad C_7 = \frac{Gr_c(2\theta_i+1)}{6\,Re}\ ,$$

$$C_8 = \frac{2U_i s^2 + 2M\Gamma - 2M\,\frac{Gr_p}{Re}\theta_i}{2S^2\,sinh(S/2)},\qquad C_9 = \frac{M(\frac{Gr_p}{\mathrm{Re}} - 2\Gamma)}{2S^2\sinh(S/2)},\qquad C_{10} = -\frac{M\,\frac{Gr_p}{\mathrm{Re}}(-2\theta_i+1)}{S^2},$$

$$C_{11} = -\frac{M\Gamma - 2M\,\frac{Gr_p}{\mathrm{Re}}\theta_i - M\,\frac{Gr_p}{2\,\mathrm{Re}}}{S^2}$$

$$C_{12} = 1152MS^5 - 96M^2\frac{Gr_c}{\mathrm{Re}}S^3 - 144M^2\frac{Gr_p}{\mathrm{Re}}S^3 + M\frac{Gr_c}{\mathrm{Re}}S^5 + 2304M^2\frac{Gr_p}{\mathrm{Re}}S$$
$$+ 48M\frac{Gr_p}{\mathrm{Re}}S^3 + 2M\frac{Gr_c}{\mathrm{Re}}\theta_i S^5 - 4608M^2\frac{Gr_p}{\mathrm{Re}}\theta_i S - 96M\frac{Gr_p}{\mathrm{Re}}\theta_i S^3 + 384M^2\frac{Gr_c}{\mathrm{Re}}\theta_i S^3$$
$$- 288M^2\frac{Gr_p}{\mathrm{Re}}\theta_i S^3$$

$$C_{13} = 24M(\frac{Gr_c}{Re}s^4 - 768M\frac{Gr_p}{Re} + 1536M\frac{Gr_p}{Re}\theta_i + 32M\frac{Gr_c}{Re}s^2 - 2\frac{Gr_c}{Re}\theta_i s^4 + 4\frac{Gr_p}{Re}\theta_i s^4$$
$$- 128M\frac{Gr_c}{Re}\theta_i s^2 + 192M\frac{Gr_p}{Re}\theta_i s^2)(sinh(s/4))^2 + 2\frac{Gr_p}{Re}\theta_i s^4 - 48M\frac{Gr_p}{Re}s^2$$
$$- \frac{Gr_p}{Re}s^4 + 96M\frac{Gr_p}{Re}\theta_i s^2$$

$$C_{14} = -1152\frac{Gr_p}{Re}S(2\theta_i - 1)M^2,\ C_{15} = 24S^6 + 2304MS^4 - 9216M^2S^2$$

$$C_{16} = -4608MS^3 + 384MS^5 + 4608M^2S^3\ ,\ C_{17} = 18432M^2s^2 - 2304Ms^4$$

$$C_{18} = -3M\frac{Gr_p}{\mathrm{Re}}S + 24Ms^3 + 3M\frac{Gr_c}{16\,\mathrm{Re}}S^3 - 3M^2\frac{Gr_p}{\mathrm{Re}}S - 5M\frac{Gr_c}{8\,\mathrm{Re}}\theta_i S^3$$
$$- 6M^2\frac{Gr_p}{\mathrm{Re}}\theta_i S + 6M\frac{Gr_p}{\mathrm{Re}}\theta_i S$$

$$C_{19} = \cosh(S/2)\left(\frac{Gr_c S^4}{32\,\mathrm{Re}} + 12S^4 - 12M\frac{Gr_p}{\mathrm{Re}} + 48M\frac{Gr_p}{\mathrm{Re}}\theta_i + 24M^2\frac{Gr_p}{\mathrm{Re}}\theta_i\right.$$
$$\left. + M\frac{Gr_c S^2}{2\,\mathrm{Re}} - 3M\frac{Gr_p S^2}{2\,\mathrm{Re}} - \frac{Gr_c\theta_i S^4}{16\,\mathrm{Re}} - 4M\frac{Gr_c\theta_i S^2}{\mathrm{Re}} - 6M\frac{Gr_p}{\mathrm{Re}}\theta_i S^2\right) + 12M\frac{Gr_p}{\mathrm{Re}}$$
$$+ 24M^2\frac{Gr_p}{\mathrm{Re}}\sinh(S/4)^2 - 24M\frac{Gr_p}{\mathrm{Re}}\theta_i - M\frac{Gr_c S^2}{2\,\mathrm{Re}} + 3M\frac{Gr_p S^2}{2\,\mathrm{Re}} + 2M\frac{Gr_c}{\mathrm{Re}}\theta_i S^2$$

$$C_{20} = 12M\frac{Gr_p}{\mathrm{Re}}S\sinh(S/4)^2 + 6M\frac{Gr_p}{\mathrm{Re}}S$$
$$C_{21} = +12MS + 24M^2\sinh(S/2) - \frac{S^4\sinh(S/2)}{8} - 12MS^2\sinh(S/2),$$
$$+ 24MS\sinh(S/4)^2$$
$$C_{22} = -12M^2S - MS^3,\ C_{23} = 48M^2\sinh(S/4)^2 - 24M^2 + 6MS^2$$

$$C_{27} = \frac{(Pe(2\theta_i C_{10} - C_{11} + C_{11}\,2\theta_i)}{2}\ \mathrm{C}_{28} = \frac{\mathrm{C}_{10}\mathrm{Pe}(-1+2\theta_\mathrm{i})}{3}\ C_{29} = \frac{C_8 Pe(1-2\theta_i)}{S^2}$$
$$C_{30} = \frac{C_9 Pe(1-2\theta_i)}{S^2}, C_{31} = \frac{2\theta_i C_8 Pe}{S}, C_{32} = \frac{2\theta_i C_9 Pe}{S}, C_{33} = \frac{C_8 Pe(1-2\theta_i)}{S},$$

$$C_{34} = \frac{C_9 Pe(1-2\theta_i)}{S}\ C_{35} = \frac{Pe(2\theta_i+1)(40C_5 + 15C_6 - 6C_7 - \frac{5\Gamma}{2} + 80U_i)}{960}$$

$$C_{36} = -\left(\frac{Pe}{S^2}\left(\frac{M\Gamma}{8} + \frac{MGr_p}{48\,\mathrm{Re}} + \frac{MGr_p\theta_i}{24\,\mathrm{Re}} + \frac{3M\theta_i\Gamma}{4} - \frac{7MGr_p\theta_i^2}{6\,\mathrm{Re}}\right)\right)$$
$$- \frac{Pe}{S^2\sinh(S/2)}\left(\frac{2\sinh(S/2)}{S^2}\left(\frac{M\Gamma}{2} + \frac{U_i S^2}{2} - \frac{MGr_p\theta_i}{2} - M\theta_i\Gamma + \frac{MGr_p\theta_i^2}{\mathrm{Re}} - \theta_i U_i S^2\right)\right.$$
$$+ \frac{2\theta_i\cosh(S/2)}{S}\left(U_i S^2 + M\Gamma - M\frac{Gr_p}{\mathrm{Re}}\theta_i\right) - \frac{M(2\theta_i - 1)\left(\frac{Gr_p}{\mathrm{Re}} - 2\Gamma\right)}{4S} + \frac{M\theta_i\left(\frac{Gr_p}{\mathrm{Re}} - 2\Gamma\right)}{S}$$
$$\left. - \frac{\cosh(S/2)(2\theta_i - 1)(U_i S^2 + M\Gamma - M\frac{Gr_p}{\mathrm{Re}}\theta_i)}{2S}\right)$$